Chapter 5
Surface Phonons

Classical bulk solid-state physics can, broadly speaking, be divided into two categories, one that relates mainly to the electronic properties and another in which the dynamics of the atoms as a whole or of the cores (nuclei and tightly bound core electrons) is treated. This distinction between lattice dynamics and electronic properties, which is followed by nearly every textbook on solid-state physics, is based on the vastly different masses of electrons and atomic nuclei. Displacements of atoms in a solid occur much more slowly than the movements of the electrons. When atoms are displaced from their equilibrium position, a new electron distribution with higher total energy results; but the electron system remains in its ground state, such that after the initial atomic geometry has been reestablished, the whole energy amount is transferred back to the lattice of the nuclei or cores. The electron system is not left in an excited state. The total electronic energy can therefore be considered as a potential for the movement of the nuclei. On the other hand, since the electronic movement is much faster than that of the nuclei, a first approximation for the dynamics of the electrons is based on the assumption of a static lattice with fixed nuclear positions determining the potential for the electrons. This approximation of separate, non-interacting electron dynamics and lattice (nuclear/core) dynamics is called the *adiabatic approximation*. It was introduced into solid-state and molecular physics by Born and Oppenheimer [5.1]. It is clear, however, that certain phenomena, such as the scattering of conduction electrons on lattice vibrations, are beyond this approximation.

For surface, interface and thin film physics the same arguments are valid and therefore, within the framework of the adiabatic approximation, the dynamics of surface atoms (or cores) and of surface electrons can be treated independently.

The lattice vibrations of atoms near the surface are expected to have frequencies different from those of bulk vibrations since, on the vacuum side of the surface, the restoring forces are missing. The properties of surface lattice vibrations and the conditions for their existence will be the subject of this chapter. Like the corresponding bulk excitations, surface vibrations are in principle quantized, although a classical treatment is sufficient in many cases because of the relatively high atomic masses and the small energy of the resulting quanta. The quanta of surface vibrations are called *surface phonons*.

H. Lüth, *Solid Surfaces, Interfaces and Thin Films*, 5th ed., Graduate Texts in Physics,
DOI 10.1007/978-3-642-13592-7_5,

In contrast to bulk solid-state physics, for surfaces, the distinction between surface lattice dynamics and surface electronic states is not a sufficient classification. Surface physics treats not only clean surfaces, but also surfaces with well-defined adsorbates. Surface physics therefore includes, besides the electron and lattice dynamics of the clean surface, a third important field, that of surfaces with adsorbed molecules or atoms (Chap. 10). For these systems one can also apply the adiabatic approximation, i.e., the vibrations and electronic states of an adsorbed atom or molecule can be considered separately. The same is true for the interface layer between two solids, e.g., a semiconductor film epitaxially grown on a different semiconductor substrate. At the interface itself the atoms of the two "touching" materials display characteristic vibrational and electronic properties.

5.1 The Existence of "Surface" Lattice Vibrations on a Linear Chain

As in the bulk case, the essential characteristics of surface lattice dynamics can be demonstrated using the simple model of a diatomic linear chain (Fig. 5.1). A model for the surface of a 3D solid is then obtained by arranging an infinite number of chains with their axes normal to the surface in a regular array, i.e. with 2D translational symmetry parallel to the surface (Fig. 5.2). In the present context the chains are not extended over the whole infinite space – as in the bulk case, but they end at the surface (semi-infinite case). Nevertheless, to a rough approximation, the dynamical equations can be assumed to be unchanged with respect to those of an infinite chain:

$$M\ddot{s}_n^{(1)} = f(s_n^{(2)} - s_n^{(1)}) - f(s_n^{(1)} - s_{n-1}^{(2)}),$$

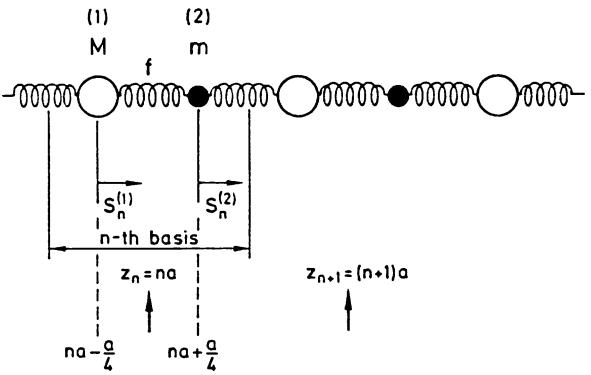

Fig. 5.1 The model of a diatomic linear chain with two different atomic masses $M(1)$ and $m(2)$. A single restoring force f is assumed between the masses. The position of the nth unit cell is described by its geometrical centre $z_n = na$; the displacements of the two atoms in the nth unit cell from equilibrium are $s_n^{(1)}$ and $s_n^{(2)}$

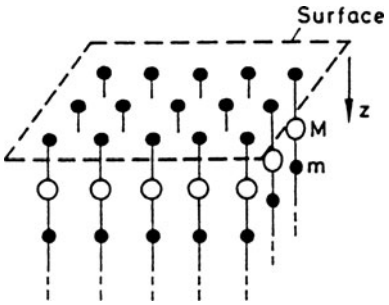

Fig. 5.2 2D arrangement of diatomic linear chains with translational symmetry in the surface. This model shows some characteristics of surface lattice dynamics

i.e.

$$M\ddot{s}_n^{(1)} = -f(2s_n^{(1)} - s_n^{(2)} - s_{\mathrm{n-1}}^{(2)}), \tag{5.1a}$$

$$m\ddot{s}_n^{(2)} = -f(2s_n^{(2)} - s_{n+1}^{(1)} - s_n^{(1)}). \tag{5.1b}$$

Changes of force constants and reconstructions at the surface are not considered in this simple model.

The plane-wave ansatz

$$s_n^{(1)} = M^{-1/2}c_1 \exp\left\{\mathrm{i}\left[ka\left(n - \frac{1}{4}\right) - \omega t\right]\right\}, \tag{5.2a}$$

$$s_{\mathrm{n}}^{(2)} = m^{-1/2}c_2 \exp\left\{\mathrm{i}\left[ka\left(n + \frac{1}{4}\right) - \omega t\right]\right\}, \tag{5.2b}$$

leads to the equations

$$-\omega^2 M^{1/2}c_1 = -fc_1 M^{-1/2} + 2fc_2 m^{-1/2}\cos\frac{ka}{2}, \tag{5.3a}$$

$$-\omega^2 m^{1/2}c_2 = -fc_2 m^{-1/2} + 2fc_1 M^{-1/2}\cos\frac{ka}{2}, \tag{5.3b}$$

which, for an infinite chain, have the solutions:

$$\omega_{\pm}^2 = \frac{f}{Mm}\left[(M+m) \pm \sqrt{(M+m)^2 - 2Mm(1-\cos ka)}\right]. \tag{5.4}$$

The frequencies $\omega_-(k)$ and $\omega_+(k)$ correspond to the well-known acoustic and optic dispersion branches of lattice waves for the infinite chain (Fig. 5.3).

For surfaces, one may modify the model in the following way. The chain is terminated at one end, but extends to infinity in the other direction. Therefore, far away from the free end, approximately the same solutions exist as for the infinite chain. Furthermore, real lattice vibrations have, in any case, a finite correlation length because of anharmonic interactions. We now seek new solutions to (5.1–5.3) which

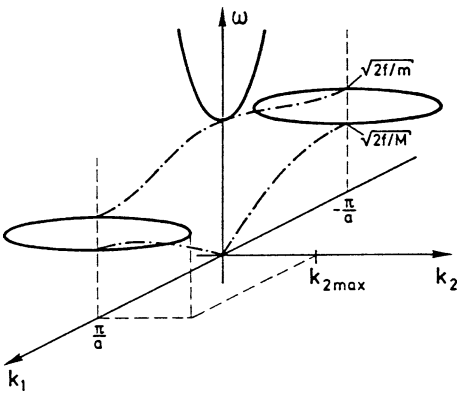

Fig. 5.3 Dispersion branches for "bulk" (dash-dotted) and "surface" (dashed) lattice vibrations (phonons) of a semi-infinite diatomic chain (atomic masses M, m; restoring force f). k_1 and k_2 are the real and imaginary parts of the complex wavevector, i.e., k_2 is the exponential decay constant of the "surface" phonons

are localized near the end of the chain, i.e., which have a negligible vibrational amplitude far away from the end of the chain in the bulk. This can be achieved by considering waves whose amplitude decays exponentially away from the end of the chain. For this purpose we make an ansatz with a complex wave vector

$$\tilde{k} = k_1 + \mathrm{i}k_2, \tag{5.5}$$

but we require the frequencies ω to be real. Is it possible to solve (5.4) with real $\omega_\pm$ but with complex $\tilde{k}$? The imaginary part k_2 would lead to exponentially decaying waves as required. Using the relations

$$\cos(\mathrm{i}z) = \cosh(z), \;\; \sin(\mathrm{i}z) = \mathrm{i}\sinh(z), \tag{5.6}$$

we can express $\cos(ka)$ in (5.4) as

$$\cos(\tilde{k}a) = \cos(k_1 a)\cosh(k_2 a) - \mathrm{i}\sin(k_1 a)\sinh(k_2 a). \tag{5.7}$$

Because of the reality condition on $\omega_\pm$, $\mathrm{Im}\{\cos(\tilde{k}a)\}$ in (5.7) must vanish, i.e.,

$$\mathrm{Im}\{\cos(\tilde{k}a)\} = \sin(k_1 a)\sinh(k_2 a) = 0. \tag{5.8}$$

The solution with $k_2 = 0$ yields the bulk dispersion branches (5.4). For the surface solutions we require

$$k_2 \neq 0 \text{ and } k_1 a = n\pi \text{ with } n = 0, \pm 1, \pm 2, \ldots. \tag{5.9}$$

We are interested in solutions for the first bulk Brillouin zone and therefore consider the cases $n = 0$, 1, i.e.,

$$\cos(\tilde{k}a) = \cos(n\pi)\cosh(k_2 a) = (-1)^n \cosh(k_2 a); \;\; n = 0, 1. \tag{5.10}$$

The possible frequencies of surface solutions are therefore

$$\omega_{\pm}^2 = \frac{f}{Mm}\left\{(M+m) \pm \sqrt{(M+m)^2 - 2Mm[1-(-1)^n \cosh(k_2 a)]}\right\}, \quad (5.11)$$

where the quantity under the square-root sign must be positive because we require real $\omega_{\pm}^2$ values. The solution with $n = 0$, i.e., $k_1 = 0$ at the Γ-point of the Brillouin zone (in k_1) is

$$\omega^2(k_1 = 0, k_2) = \frac{f}{Mm}\left[(M+m) + \sqrt{(M+m)^2 - 2Mm[1-\cosh(k_2 a)]}\right]. \quad (5.12)$$

Since $[1 - \cosh(k_2 a)]$ is negative for all $k_2 a$, there is no restriction on k_2, but only the positive square root in (5.12) is a solution. The curvature of (5.12) with respect to k_2 is always positive and the value of $\omega(k_1 = 0, k_2 = 0)$ equals that of the bulk optical branch $[2f(1/M + 1/m)]^{1/2}$ at Γ. Figure 5.3 shows that at $\Gamma(k_1 = 0)$ these surface solutions are possible with frequencies above the maximum bulk phonon frequency.

The solutions of (5.11) with $n = 1$, i.e., $k_1 = \pi/a$, are located in k-space at the Brillouin-zone boundary. The condition for a real square root now reads

$$|k_2| < \frac{1}{a}\operatorname{arc\,cosh}\frac{M^2 + m^2}{2Mm} \equiv k_{2\max}. \quad (5.13)$$

Thus there exist the solutions

$$\omega_{\pm}^2(k_1 = \pi/a, k_2) = \frac{f}{Mm}\left\{(M+m) \pm \sqrt{(M+m)^2 - 2Mm[1+\cosh(k_2 a)]}\right\} \quad (5.14)$$

only for a limited range of k_2 values (5.13). For $k_2 = 0$ the solutions are

$$\omega_+(k_2 = 0) = (2f/m)^{1/2} \text{ and } \omega_-(k_2 = 0) = (2f/M)^{1/2}. \quad (5.15a)$$

At the maximum value $k_{2\,\max}$ one obtains

$$\omega_{\pm}(k_2 = k_{2\max}) = \sqrt{f(1/M + 1/m)}. \quad (5.15b)$$

Both branches $\omega_{\pm}$ are continuous at $k_{2\max}$ and have frequencies at $k_2 = 0$ that are identical to those of the bulk acoustic and optical lattice vibrations at the zone boundary. The possible surface vibrational frequencies fill the range between the acoustic and optical branches of the bulk excitations (Fig. 5.3). Boundary conditions at the surface impose further restrictions (Sect. 5.2).

The possible displacements of atom i in the "surface" modes follow according to (5.2) as

$$s_n^{(i)} = C_i \exp[\mathrm{i}(\tilde{k} z_n^i - \omega t)], \tag{5.16}$$

where

$$z_n^i = a\left(n - \frac{1}{4}\right) \text{ for atom } (1) = (i), \text{ and } a\left(n + \frac{1}{4}\right) \text{ for atom } (2) = (i)$$

are the corresponding atomic coordinates. From Fig. 5.3 one sees that $\tilde{k}$ can have the values

$$\tilde{k} = k_1 + \mathrm{i}k_2 = \pm\pi/a + \mathrm{i}k_2 \tag{5.17}$$

at the Γ-point ($k_1 = 0$) and at the boundaries of the Brillouin zone, respectively. Apart from different, constant phase factors all these solutions are vibrations of the form

$$s_n^{(\mathrm{i})} \propto \exp(-k_2 z_n^{(\mathrm{i})}) \mathrm{e}^{-\mathrm{i}\omega t}, \; k_2 > 0, \tag{5.18}$$

whose vibrational amplitude decays exponentially away from the end of the chain, i.e. the surface at $z = 0$, into the interior of the chain.

5.2 Extension to a Three-Dimensional Solid with a Surface

Qualitatively, it is relatively easy to extend the above arguments to the case of a 3D solid with a surface. This is illustrated in Fig. 5.2 where the finite solid is modelled by a regular array of parallel, semi-infinite chains. This model is only realistic in cases where the chemical bonds in directions parallel to the surface are weak, i.e., for strongly anisotropic solids. Nevertheless, we can use it to provide a qualitative idea for the features associated with general surface vibrational modes.

For every chain we have the possible vibrational modes (5.18) discussed above. However, different chains might vibrate with different phases. Due to the weak interaction between the chains the phases are correlated with each other. The phase difference can be described by a wave vector $\boldsymbol{k}_\parallel$ parallel to the surface. Since we are interested in wave propagation parallel to the surface, the wave vector of a general 3D-lattice vibration

$$\boldsymbol{s}_{\boldsymbol{k}}(\boldsymbol{r}) = A\hat{\boldsymbol{e}}_{\boldsymbol{k}} \mathrm{e}^{\mathrm{i}(\boldsymbol{k}\cdot\boldsymbol{r} - \omega t)} \tag{5.19}$$

can be split up into a part parallel to the surface $\boldsymbol{k}_\parallel$ describing the plane wave moving parallel to the surface, and a part $k_\perp$ normal to the surface. With $\boldsymbol{k} = \boldsymbol{k}_\parallel + \boldsymbol{k}_\perp$ and $\boldsymbol{r} = \boldsymbol{r}_\parallel + \hat{\boldsymbol{e}}_z z$, (5.19) yields

$$\boldsymbol{s}_{\boldsymbol{k}}(\boldsymbol{r}) = A\hat{\boldsymbol{e}}_{\boldsymbol{k}} \exp[\mathrm{i}(\boldsymbol{k}_\parallel \cdot \boldsymbol{r}_\parallel + k_\perp z - \omega t)]. \tag{5.20a}$$

Parallel to the surface plane waves with real $\boldsymbol{k}_\parallel$ are possible, but normal to the surface only solutions of the type (5.18) with imaginary $k_\perp = \mathrm{i}k_2$ need be considered. The decay constant k_2 is often designated by $\kappa_\perp$. One obtains the following general form for a surface lattice vibration:

$$\boldsymbol{s}_{\boldsymbol{k}_\parallel,\kappa_\perp} = A\hat{\boldsymbol{e}}_{\boldsymbol{k}_\parallel,\kappa_\perp} \mathrm{e}^{-\kappa_\perp z} \exp[\mathrm{i}(\boldsymbol{k}_\parallel \cdot \boldsymbol{r}_\parallel - \omega t)]. \tag{5.20b}$$

Equation (5.20b) is only valid for primitive unit cells; if there is more than one atom per unit cell, an additional index (i) as in (5.18) describes the particular type of atom.

A surface vibrational mode is therefore characterized by its frequency ω (or quantum energy $\hbar\omega$), its wave vector $\boldsymbol{k}_\parallel$ parallel to the surface, and the decay constant $\kappa_\perp$, which determines the decay length of the vibrational amplitude from the surface into the interior of the crystal. These quantities are not independent of one another. They are related via the dynamical equations (as in the 3D bulk case) and via the boundary condition that no forces should act from the vacuum side on the topmost layer of surface atoms. Thus from the "continuous" spectrum of possible surface-mode frequencies between the acoustic and optical bulk modes and above (Fig. 5.3) these restrictions select (for a primitive unit cell) one particular frequency ω for each $\boldsymbol{k}_\parallel$ and $\kappa_\perp$. For a crystal with two atoms per unit cell both an acoustic and an optical surface phonon branch exist.

In analogy to the bulk case, surface phonons can therefore be described by a 2D dispersion relation $\omega(\boldsymbol{k}_\parallel, \kappa_\perp)$. The function $\omega(\boldsymbol{k}_\parallel, \kappa_\perp)$ is periodic in 2D reciprocal space. The usual way to display the dispersion relation $\omega(\boldsymbol{k}_\parallel, \kappa_\perp)$ is by plotting the function $\omega(\boldsymbol{k}_\parallel)$ along certain symmetry lines of the 2D Brillouin zone (Fig. 5.4). In

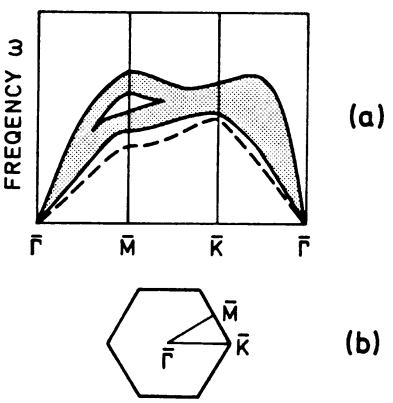

Fig. 5.4 Qualitative picture of a 2D surface phonon dispersion relation (**a**) along the symmetry lines $\overline{\Gamma M}$, $\overline{MK}$ and $\overline{K\Gamma}$ of the 2D surface Brillouin zone of a *hexagonal* (111) surface of a fcc lattice (**b**). The surface phonon dispersion is given by the dashed line in (**a**). The shaded area indicates the range of bulk phonon frequencies at all possible $k_\perp$ wave vectors for $k_\parallel$ values on the symmetry lines

these plots it is usual to show the bulk phonons, too, since they also contribute to the possible modes close to the surface. For a particular surface, all bulk modes with a certain $\boldsymbol{k}_{\parallel}$ have to be taken into account. The projection of the bulk modes at a fixed $\boldsymbol{k}_{\parallel}$ and for all $\boldsymbol{k}_{\perp}$ yields in the 2D plot (Fig. 5.4) a continuous area of possible $\omega(\boldsymbol{k}_{\parallel})$ values. In order to generate plots such as Fig. 5.4 one has to project the 3D bulk dispersion branches onto the particular 2D surface Brillouin zone; i.e. certain bulk directions and points of high symmetry in the 3D Brillouin zone are projected onto the 2D surface zone. How this is done for some low-index faces of common 3D lattices is depicted in Figs. 5.5–5.7.

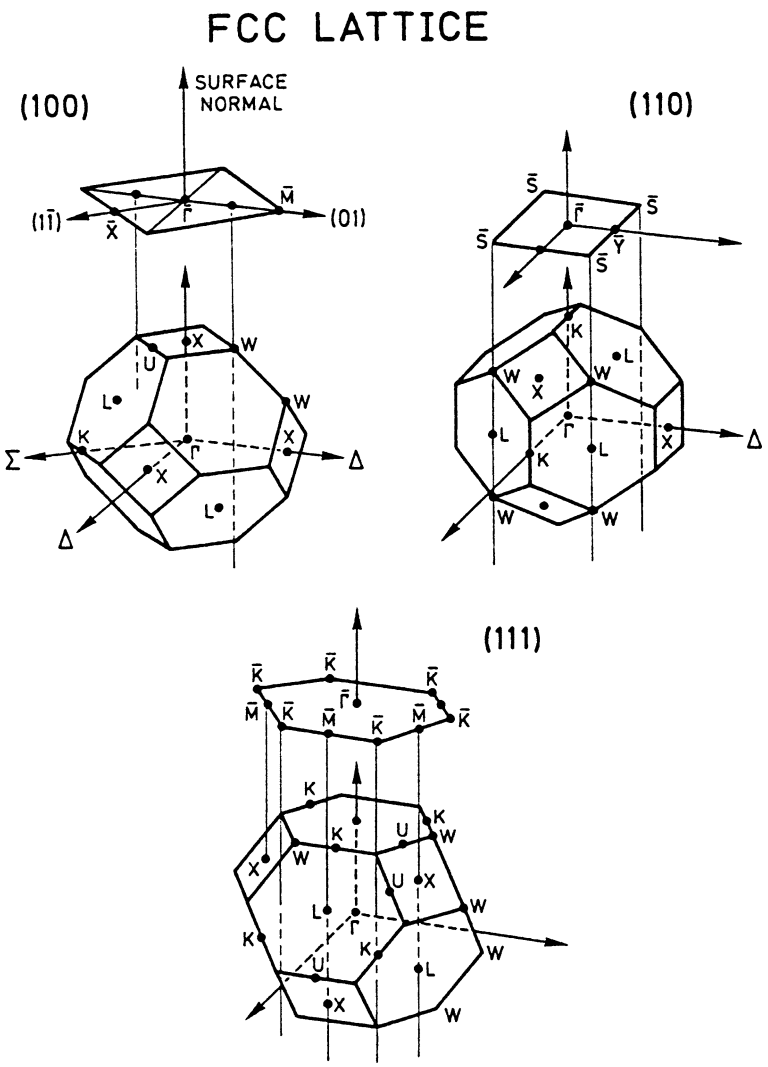

Fig. 5.5 Relation between the 2D surface Brillouin zones of the (100), (111) and (110) surfaces of a fcc lattice and the bulk Brillouin zone

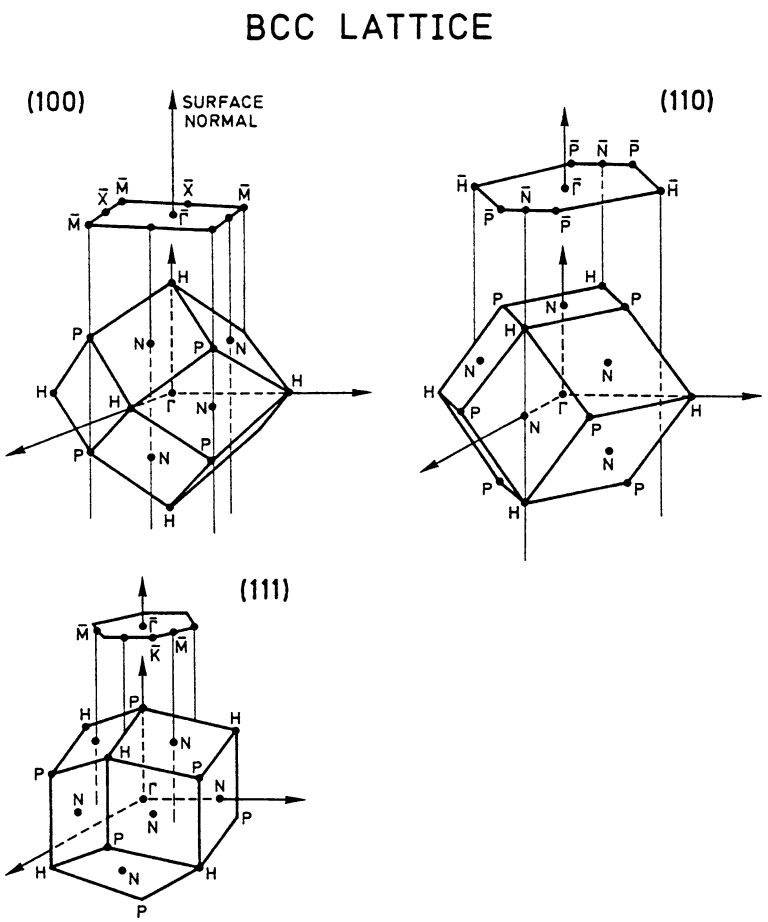

Fig. 5.6 Relation between the 2D surface Brillouin zones of the (100), (111) and (110) surfaces of a bcc lattice and the bulk Brillouin zone

It is worth mentioning that a more rigorous treatment of surface lattice dynamics [5.2] leads to a simple scaling rule which connects the decay length $\kappa_\perp$ of the vibrational amplitude of a surface phonon to its wave vector $k_\parallel$: in the non-dispersive regime where $\mathrm{d}\omega/\mathrm{d}k_\parallel$ is constant, i.e., for small wave vectors $k_\parallel$, the decay constant $\kappa_\perp$ is proportional to $k_\parallel$; the longer the wavelength of the surface vibration, the deeper its vibrational amplitude extends into the solid.

Similar considerations as applied here to the solid–vacuum interface lead, for the solid–solid interface, e.g. at an epitaxially grown semiconductor overlayer (Chap. 8), to the existence of interface phonons. Their vibrational amplitude decays exponentially into each solid on both sides of the interface [5.3].

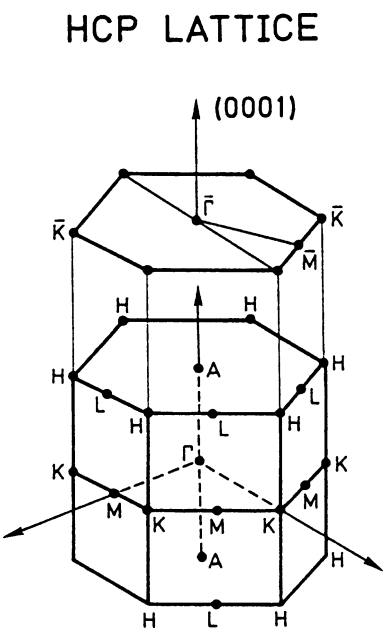

Fig. 5.7 Relation between the (0001) surface Brillouin zone of a hcp lattice and the corresponding bulk Brillouin zone

5.3 Rayleigh Waves

In the study of bulk solids the dispersionless part of the acoustic phonons was well known as sound waves long before the development of lattice dynamics [5.4]. Debye used this well-known part of the phonon spectrum to evaluate his approximation for the lattice specific heat. A similar situation holds for the dispersionless low-frequency part of the surface phonon dispersion branches. Part of these surface phonon modes were already known in 1885 as Rayleigh surface waves of an elastic continuum filling a semi-infinite halfspace [5.5, 5.6]. In classical continuum theory one can only describe lattice vibrations whose wavelength is long compared to the interatomic separation. A macroscopic deformation of a solid continuum can therefore be described in terms of displacements of volume elements $\mathrm{d}v$ whose dimensions are large in relation to interatomic distances, but small in comparison with the macroscopic body. The important variables in this sense are the displacements $\boldsymbol{u} = \boldsymbol{r}' - \boldsymbol{r}$ of these volume elements $\mathrm{d}v$ and the strain tensor

$$\epsilon_{ij} = \frac{1}{2}\left(\frac{\partial u_j}{\partial x_i} + \frac{\partial u_i}{\partial x_j}\right). \tag{5.21}$$

In the elastic regime ϵ_{ij} is related to the stress field $\sigma_{kl} = \partial F_k/\partial f_l$ (force in k direction per area element in l direction) via the elastic compliances

$$\epsilon_{ij} = \sum_{kl} S_{ijkl}\sigma_{kl}. \tag{5.22}$$

In this continuum model the time variation and spatial structure of an elastic wave can be given in terms of the displacement field $\boldsymbol{u}(\boldsymbol{r}, t)$ which describes the microscopic movement of little volume elements containing a considerable number of elementary cells (Note that in the long-wavelength limit, neighboring elementary cells behave identically). The Rayleigh waves that are solutions of the wave equation for an elastic continuous half-space are obtained in the following way: every vector field – including the displacement field $\boldsymbol{u}(\boldsymbol{r}, t)$ – can be split up into a turbulence-free and a source-free part $\boldsymbol{u}'$ and $\boldsymbol{u}''$:

$$\boldsymbol{u} = \boldsymbol{u}' + \boldsymbol{u}'' \tag{5.23a}$$

with

$$\mathrm{curl}\boldsymbol{u}' = \boldsymbol{0} \text{ and } \mathrm{div}\boldsymbol{u}'' = 0. \tag{5.23b}$$

In the bulk, differential wave equations can be solved for both contributions giving longitudinal sound waves $[\boldsymbol{u}'(\boldsymbol{r}, t)]$ and transverse (shear) sound waves $[\boldsymbol{u}''(\boldsymbol{r}, t)]$ with the sound velocities c_1 and c_2, respectively. In the present situation of a semi-infinite halfspace we assume a coordinate system as shown in Fig. 5.8, and try solutions that are dependent only on x ($\parallel$ to the surface) and z ($\perp$ to the surface). Because of (5.23b) we can introduce two new functions ϕ and ψ which have the character of potentials

$$\boldsymbol{u}' = -\mathrm{grad}\phi, \tag{5.24}$$

$$u_x'' = -\frac{\partial\psi}{\partial z},\ u_z'' = \frac{\partial\psi}{\partial x}. \tag{5.25}$$

The definition (5.25) is possible because

$$\mathrm{div}\boldsymbol{u}'' = \frac{\partial u_x''}{\partial x} + \frac{\partial u_z''}{\partial z} = 0. \tag{5.26}$$

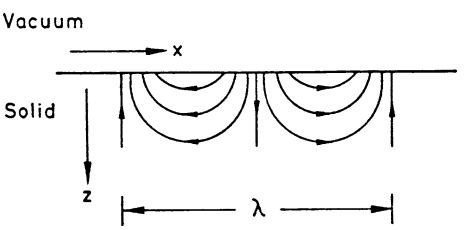

Fig. 5.8 Displacement field $\boldsymbol{u}(\boldsymbol{r}, t)$ (instantaneous picture) of a Rayleigh surface wave travelling in the x-direction along the boundary of a semi-infinite continuous solid half space

Instead of treating the displacement field $\boldsymbol{u}(\boldsymbol{r}, t)$ directly, we can use the functions $\phi(x, z)$ and $\psi(x, z)$. The function ϕ describes longitudinal excitations, whereas ψ is related to the transverse part of the displacement field. The general equations of motion for an isotropic, 3D bulk, elastic solid can be reduced to wave equations for the generalized potentials ϕ and ψ. In analogy to the bulk problem we therefore try to solve the following wave equations for the semi-infinite halfspace:

$$c_{\mathrm{l}}^{1/2} \frac{\partial^2 \phi}{\partial t^2} - \Delta\phi = 0, \quad c_{\mathrm{t}}^{1/2} \frac{\partial^2 \psi}{\partial t^2} - \Delta\psi = 0. \tag{5.27}$$

In accordance with the character of ϕ and ψ (5.27) contains the longitudinal and the transverse sound velocities c_{l} and c_{t}. For the solution of (5.27) we try the ansatz of surface waves travelling parallel to the surface along x with an amplitude dependent on z ($\boldsymbol{u}$ must vanish for $z \to \infty$):

$$\phi(x, z) = \xi(z)\mathrm{e}^{\mathrm{i}(kx-\omega t)}, \ \ \psi(x, z) = \eta(z)\mathrm{e}^{\mathrm{i}(kx-\omega t)}. \tag{5.28}$$

From (5.27) it then follows that

$$\xi'' - p^2\xi = 0 \quad \text{with } p^2 = k^2 - (\omega/c_{\mathrm{l}})^2, \tag{5.29a}$$

$$\eta'' - q^2\eta = 0 \quad \text{with } q^2 = k^2 - (\omega/c_{\mathrm{t}})^2. \tag{5.29b}$$

For $p^2 > 0$ and $q^2 > 0$, the amplitudes ξ and η are clearly exponential functions that decay into the bulk of the material as

$$\xi = A\mathrm{e}^{-pz}, \quad \eta = B\mathrm{e}^{-qz}. \tag{5.30}$$

The final solutions have the character typical of surface excitations (5.20b):

$$\phi = A\mathrm{e}^{-pz}\mathrm{e}^{\mathrm{i}(kx-\omega t)} \quad \text{with } p = \sqrt{k^2 - (\omega/c_{\mathrm{l}})^2}, \tag{5.31a}$$

$$\psi = B\mathrm{e}^{-qz}\mathrm{e}^{\mathrm{i}(kx-\omega t)} \quad \text{with } q = \sqrt{k^2 - (\omega/c_{\mathrm{t}})^2}. \tag{5.31b}$$

The displacement field $(u_x, 0, u_z)$ is then derived from (5.24 and 5.25) by differentiation of (5.31):

$$u_x = -\frac{\partial\phi}{\partial x} - \frac{\partial\psi}{\partial z}, \quad u_z = -\frac{\partial\phi}{\partial z} + \frac{\partial\psi}{\partial x}. \tag{5.32}$$

From (5.32) we see that the displacement field of the surface excitation contains both a longitudinal and a transverse contribution; the wave is of mixed longitudinal-transverse character and its velocity must thus depend on both c_{l} and c_{t}. For the further evaluation of the Rayleigh wave phase velocity ω/k we use the boundary condition that at the very surface ($z = 0$) there is no elastic stress, i.e.,

$$\sigma_{zz}|_{z=0} = \sigma_{yz}|_{z=0} = \sigma_{xz}|_{z=0} = 0. \tag{5.33}$$

In the subsequent somewhat tedious calculation [5.6], the elastic constants enter via (5.21 and 5.22). But even with the assumption of incompressibility for the semi-infinite continuum only an approximate solution is possible. One obtains the phase velocity of the Rayleigh wave as

$$c_{\mathrm{RW}} \simeq (1 - 1/24)c_{\mathrm{t}} \tag{5.34}$$

and the direct relations between its wave vector k and the parameters p and q

$$p \simeq k,\ q \simeq k(12)^{-1/2}. \tag{5.35}$$

From (5.34) we see that the phase velocity of Rayleigh surface waves is even lower than the transverse sound velocity [5.5, 5.6]; this is also true for cubic crystals. Figure 5.8 illustrates qualitatively the spatial structure of the displacement field of a Rayleigh wave with wavelength $\lambda = 2\pi/k$. The mixed longitudinal-transverse character is seen from the direction of the displacements which are partially parallel and partially normal to the propagation direction x.

It should also be emphasized that the treatment in this section is based on the continuum case in which the neglect of atomic structure leads to a Rayleigh wave that shows no dispersion (like for bulk sound waves). Extending the analysis to an atomically structured medium like a crystal, the surface phonon branches will show dispersion, in particular near the Brillouin-zone boundary. In Fig. 5.4 the dispersion branch indicated by the dashed line qualitatively, reflects what one can expect for Rayleigh surface phonons. Some results from experiments and more realistic calculations are presented in Sect. 5.6.

5.4 The Use of Rayleigh Waves as High-Frequency Filters

Experimentally, Rayleigh waves can be excited by a variety of methods. In principle one has to induce an elastic surface strain of adequate frequency. Atomic and molecular beam scattering (Panel X: Chap. 5) can be used, as can Raman scattering, in particular at low frequencies with high resolution, i.e., Brillouin scattering. For piezoelectric crystals and ceramics there is a particularly convenient way to excite Rayleigh waves. These materials are characterized by an axial crystal symmetry. Stress along such an axis produces an electric dipole moment in each unit cell of the crystal due to an unequal displacement of the different atoms in the cell. Simple examples are the wurtzite structure of ZnO which is built up along its hexagonal c-axis by double layers of Zn and O ions. Stress along the c-axis displaces the Zn and O lattice planes by different amounts and a dipole moment in the c-direction results. Other examples are the wurtzitic group III-nitrides (GaN, AlN, InN) and generally the III-V semiconductors that crystallize in the zinc-blende structure with an axial symmetry along the four {111} cubic cell diagonals. For practical purposes

quartz and specially designed titanate ceramics are important. A general description of the piezoelectric effect may be given in terms of the third rank piezoelectric tensor d_{ijk} which relates a polarization P_i to a general mechanical stress ϵ_{jk}

$$P_i = \sum_{jk} d_{ijk}\epsilon_{jk}, \quad \epsilon_{ij} = \sum_{k} \bar{d}_{ijk}\mathcal{E}_k. \tag{5.36}$$

Equation (5.36b) with the so-called inverse piezoelectric tensor $\bar{d}_{ijk}$ describes the inverse phenomenon by which an electric field $\mathcal{E}$ applied in a certain direction produces a mechanical strain ϵ_{ij} in such crystals. On surfaces of piezoelectric crystals the mechanical strain associated with Rayleigh waves can thus be induced by appropriately chosen electric fields; these are applied by evaporated metal grids (Fig. 5.9). A high-frequency voltage $U_\mathrm{i}(\omega)$ applied to the left-hand grids in Fig. 5.9a gives rise via (5.36) to a surface strain field, which varies harmonically in time with frequency ω and has a wavelength λ determined by the grid geometry. If ω and λ (i.e., ω and $k = 2\pi/\lambda$) are values which fall on the dispersion curve for Rayleigh waves of that material, such surface waves are excited. They travel along the surface and excite a corresponding time-varying polarization which produces an electric signal in the right-hand grid structure. The grid geometry determines a fixed wavelength λ_0. Because of the single-valued dispersion relation for surface Rayleigh waves this λ_0 allows only a particular frequency ω_0 for the surface phonons. High-frequency signals $U_\mathrm{i}(\omega_0)$ can pass the device and appear as an output signal $U_\mathrm{f}(\omega_0)$ only if $\omega_0(2\pi/\lambda_0)$ is a particular point on the Rayleigh dispersion curve (Fig. 5.9b). This dispersion curve and the geometry of the grids (equal for antenna and receiver) therefore determine the pass frequency of the filter. To give a numerical example: grids with rod distances in the 100 μm range can easily be evaported. For a Rayleigh

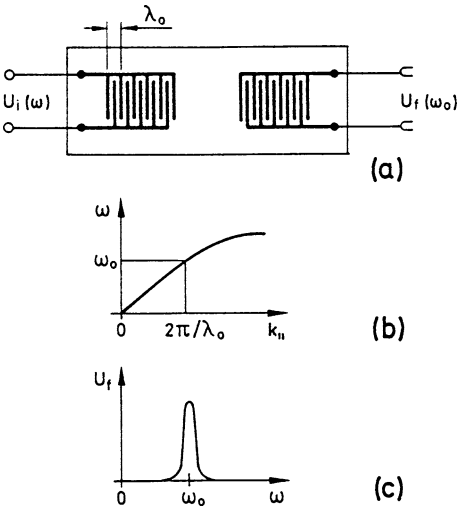

Fig. 5.9 (**a**) Schematic drawing of a Rayleigh-wave high-frequency filter. Two sets of metallic grids are evaporated onto a piezoelectric plate. The rod spacing λ_0 determines the wavevector $k_0 = 2\pi/\lambda_0$ of the excited surface wave. (**b**) Through the Rayleigh-wave dispersion relation the frequency ω_0 is fixed by λ_0. (**c**) If a continuous spectrum is fed in as input voltage $U_\mathrm{i}(\omega)$, only a sharp band $U_\mathrm{f}(\omega_0)$ is transmitted through the device

wave velocity of 4000 m/s we obtain a frequency of $\omega \simeq 24 \cdot 10^7\ \mathrm{s}^{-1}$ or $\nu \simeq 40$ MHz. Such surface-wave devices are used, e.g., in television equipment as band-pass filters for image frequencies.

5.5 Surface-Phonon (Plasmon) Polaritons

In Sect. 5.3. we considered one limiting case of the surface-phonon spectrum, namely the nondispersive acoustic type of vibrations that are derived from the bulk sound waves. A similar treatment is possible for the long-wavelength optical phonons of an InfraRed (IR) active crystal. There is a certain type of optical surface phonon that is derived from the corresponding bulk TO and LO modes near $\boldsymbol{k} = 0$. As in the bulk, these surface modes are connected with an oscillating polarization field. Besides the dynamics of the crystal, the calculation must therefore also take into account Maxwell's equations which govern the electromagnetic field accompanying the surface vibration.

We consider a planar interface located at $z = 0$ between two non-magnetic ($\mu = 1$) isotropic media. The two media, each filling a semi-infinite halfspace, are characterized by their dielectric functions $\epsilon_1(\omega)$ for $z > 0$ and $\epsilon_2(\omega)$ for $z < 0$, respectively. The dynamics of the two media is contained in their dielectric functions; the IR activity, for example, can be expressed in terms of an oscillator type $\epsilon(\omega)$ with ω_{TO} as resonance frequency (TO denotes the transverse optical phonon at Γ). The particular case of a clean surface in vacuum is contained in our analysis for $\epsilon_2 = 1$ (or $\epsilon_1 = 1$). In general, electromagnetic waves propagating inside a non-magnetic ($\mu = 1$) medium with dielectric function $\epsilon(\omega)$ obey the dispersion law (derived from the differential wave equation):

$$k^2 c^2 = \omega^2 \epsilon(\omega). \tag{5.37}$$

We look for modifications of (5.37) due to the presence of the interface. We start from the "equation of motion" for the electric field $\mathcal{E}(\boldsymbol{r}, t)$. From Maxwell's equations we obtain for a nonmetal ($\boldsymbol{j} = \boldsymbol{0}$).

$$\mathrm{curlcurl}\mathcal{E} = -\mu_0 \mathrm{curl}\dot{\boldsymbol{H}} = -\mu_0 \epsilon_0 \epsilon(\omega) \ddot{\mathcal{E}}, \tag{5.38a}$$

i.e.,

$$-c^2 \mathrm{curlcurl}\mathcal{E} = \epsilon(\omega) \ddot{\mathcal{E}}, \tag{5.38b}$$

and from charge neutrality

$$\mathrm{div}[\epsilon(\omega)\mathcal{E}] = 0. \tag{5.39}$$

Special solutions localized at the interface should be wave-like in two dimensions (parallel to the interface) with an amplitude decaying into the two media for $z \gtrless 0$:

$$\mathcal{E}_1 = \hat{\mathcal{E}}_1 \exp[-\kappa_1 z + \mathrm{i}(\boldsymbol{k}_\parallel \cdot \boldsymbol{r}_\parallel + \omega t)] \quad \text{for } z > 0, \tag{5.40a}$$

$$\mathcal{E}_2 = \hat{\mathcal{E}}_2 \exp[\kappa_2 z + \mathrm{i}(\boldsymbol{k}_\parallel \cdot \boldsymbol{r}_\parallel + \omega t)] \quad \text{for } z < 0, \tag{5.40b}$$

with $\boldsymbol{r}_\parallel = (x, y)$, $\boldsymbol{k}_\parallel = (k_x, k_y)$ parallel to the interface and $\mathrm{Re}\{\kappa_1\}, \mathrm{Re}\{\kappa_2\} > 0$. From (5.39) we obtain

$$\mathrm{i}\mathcal{E} \cdot \boldsymbol{k}_\parallel = \mathcal{E}_z \kappa, \; z \neq 0, \tag{5.41}$$

with $\kappa = \kappa_1$ and $\kappa = \kappa_2$ for media (1) and (2), respectively. Equation (5.41) excludes solutions with $\mathcal{E}$ normal to $\boldsymbol{k}_\parallel$ and $\mathcal{E}_z \neq 0$, which are localized at the interface; localized waves must be sagittal with amplitudes

$$\hat{\boldsymbol{\mathcal{E}}}_1 = \hat{\mathcal{E}}_1(\boldsymbol{k}_\parallel / k_\parallel, -\mathrm{i}k_\parallel / \kappa_1) \tag{5.42a}$$

$$\hat{\boldsymbol{\mathcal{E}}}_2 = \hat{\mathcal{E}}_2(\boldsymbol{k}_\parallel / k_\parallel, -\mathrm{i}k_\parallel / \kappa_2). \tag{5.42b}$$

If we insert the ansatz (5.40) together with the amplitudes (5.42) into (5.38b), we obtain dispersion laws similar to (5.37):

$$(k_\parallel^2 - \kappa_1^2)c^2 = \omega^2 \epsilon_1(\omega), \tag{5.43a}$$

$$(k_\parallel^2 - \kappa_2^2)c^2 = \omega^2 \epsilon_2(\omega). \tag{5.43b}$$

We now have to match the solutions $\mathcal{E}_1$ and $\mathcal{E}_2$ at the interface, i.e., we require

$$\boldsymbol{\mathcal{E}}_1^\parallel = \boldsymbol{\mathcal{E}}_2^\parallel \text{ and } \boldsymbol{D}_1^\perp = \boldsymbol{D}_2^\perp. \tag{5.44}$$

This yields

$$\hat{\boldsymbol{\mathcal{E}}}_1 = \hat{\boldsymbol{\mathcal{E}}}_2 \text{ and } \kappa_1/\kappa_2 = -\epsilon_1(\omega)/\epsilon_2(\omega). \tag{5.45}$$

Combining (5.45) with (5.43) we get the dispersion relation for surface polaritons

$$k_\parallel^2 c^2 = \omega^2 \frac{\epsilon_1(\omega)\epsilon_2(\omega)}{\epsilon_1(\omega) + \epsilon_2(\omega)}. \tag{5.46}$$

Comparing this relation with the bulk polariton dispersion (5.37) one can formally define an interface dielectric function $\epsilon_\mathrm{s}(\omega)$:

$$\frac{1}{\epsilon_\mathrm{s}(\omega)} = \frac{1}{\epsilon_1(\omega)} + \frac{1}{\epsilon_2(\omega)}. \tag{5.47}$$

From the bulk dispersion relation (5.37) we obtain the frequency of the TO bulk phonon for $k \to \infty$, i.e., for k values large in comparison with those on the light curve $\omega = ck$; ω_TO results from the pole of $\epsilon(\omega)$. Similarly we obtain the frequency ω_s of the interface waves ($k_\parallel \to \infty$) from the pole of $\epsilon_\mathrm{s}(\omega)$ (5.46, 5.47), i.e.,

$$0 = \frac{1}{\epsilon_s(\omega_s)} = \frac{\epsilon_1(\omega_s) + \epsilon_2(\omega_s)}{\epsilon_1(\omega_s)\epsilon_2(\omega_s)}, \tag{5.48a}$$

or

$$\epsilon_2(\omega_s) = -\epsilon_1(\omega_s). \tag{5.48b}$$

If we consider the special case of a crystal in vacuum, i.e. a semi-infinite halfspace with the dielectric function $\epsilon(\omega) = \epsilon_1(\omega)$ adjoining vacuum with $\epsilon_2(\omega) = 1$, the condition determining the frequency of the surface polariton is

$$\epsilon(\omega_s) = -1. \tag{5.49}$$

The simplest description of an IR-active material is in terms of an undamped oscillator-type dielectric function

$$\epsilon(\omega) = 1 + \chi_{VE} + \chi_{Ph}(\omega) \tag{5.50}$$

with

$$\chi_{VE} = \epsilon(\infty) - 1$$

and

$$\chi_{Ph} = [\epsilon(0) - \epsilon(\infty)] \frac{\omega_{TO}^2}{\omega_{TO}^2 - \omega^2},$$

where χ_{VE} describes the valence-electron contribution in terms of the high-frequency dielectric function $\epsilon(\infty)$, $\epsilon(0)$ is the static dielectric function, and ω_{TO} the frequency of the TO bulk phonons (dispersion neglected). Inserting (5.50) into (5.46) yields the dispersion relation for surface phonon polaritons:

$$\omega^2 = \frac{1}{2}\left[\omega_{LO}^2 + \left(1 + \frac{1}{\epsilon(\infty)}\right) k_\parallel^2 c^2\right] \times \left(1 - \sqrt{1 - 4\frac{[\omega_{LO}^2 + \epsilon(\infty)^{-1}\omega_{TO}^2]k_\parallel^2 c^2}{\{\omega_{LO}^2 + [1 + \epsilon(\infty)^{-1}]k_\parallel^2 c^2\}^2}}\right). \tag{5.51}$$

This dispersion is plotted in Fig. 5.10 together with the dispersion branches of the bulk IR-active TO/LO polariton branches. For large $k_\parallel$ the surface-polariton branch approaches the surface phonon frequency (ω_s) which is determined by the condition (5.49). It should be emphasized that the $k_\parallel$ range shown in Fig. 5.10 covers essentially the 10^{-3} part of the 2D Brillouin-zone diameter, i.e., for large $k_\parallel$ values in the remainder of the zone considerable dispersion might occur, but this is not contained in our simple approximation for small $k_\parallel$.

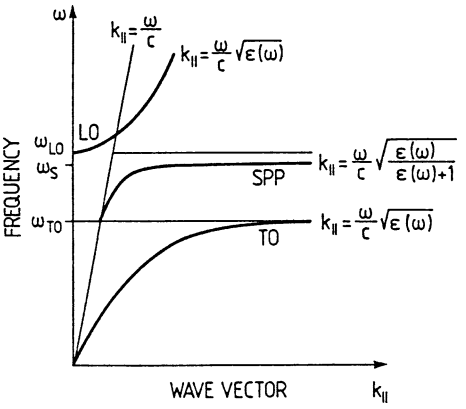

Fig. 5.10 Dispersion curve of surface phonon polaritons (SPP) of an IR active crystal together with the bulk phonon polariton curves (TO, LO) for small wave vectors parallel to the surface

It should also be noted that the analysis presented here takes into account retardation, i.e., the finite value of the light velocity c.

A much simpler derivation of the condition for the existence of optical surface phonons (5.49) and their frequency ω_s is obtained by neglecting retardation. For this purpose we ask whether there exists a wave-like solution near the interface between the IR-active crystal and the vacuum, for which both

$$\mathrm{div}\boldsymbol{P} = 0 \quad \text{for } z \neq 0, \tag{5.52a}$$

$$\mathrm{curl}\boldsymbol{P} = \boldsymbol{0} \quad \text{for } z \neq 0, \tag{5.52b}$$

with $\boldsymbol{P}$ being the polarization accompanying the lattice distortion. One should remember that for the corresponding long-wavelength bulk phonons the following conditions are valid

$$\text{TO-phonon: } \mathrm{curl}\boldsymbol{P}_{\mathrm{TO}} \neq \boldsymbol{0}, \quad \mathrm{div}\boldsymbol{P}_{\mathrm{TO}} = 0, \tag{5.53a}$$

$$\text{LO-phonon: } \mathrm{curl}\boldsymbol{P}_{\mathrm{LO}} = \boldsymbol{0}, \quad \mathrm{div}\boldsymbol{P}_{\mathrm{LO}} \neq 0. \tag{5.53b}$$

For the surface solution we require (5.52) to hold, i.e., $\mathrm{curl}\mathcal{E} = \boldsymbol{0}$ and $\mathrm{div}\mathcal{E} = 0$ (for $z \neq 0$); the electric field should therefore be derived from a potential φ:

$$\mathcal{E} = -\mathrm{grad}\varphi \tag{5.54}$$

with

$$\nabla^2\varphi = 0 \quad \text{for } z \neq 0. \tag{5.55}$$

For the solution of (5.55) we can make the ansatz of a surface wave

$$\varphi = \varphi_0 \mathrm{e}^{-k_x|z|}\mathrm{e}^{\mathrm{i}(k_x x - \omega t)}. \tag{5.56}$$

The coordinate system is that of Fig. 5.8. The wave (5.56) already fulfills (5.55) and we simply have to demand continuity for the component $D_\perp$ at the surface, $z = 0$, i.e.,

$$D_z = -\epsilon_0 \epsilon(\omega) \left.\frac{\partial \varphi}{\partial z}\right|_{z=0-\delta} = -\epsilon_0 \left.\frac{\partial \varphi}{\partial z}\right|_{z=0+\delta}. \tag{5.57}$$

This condition (5.57) is equivalent to the condition (5.49) determining the frequency of the surface polariton. According to (5.54) the electric field $\boldsymbol{\mathcal{E}} = (\mathcal{E}_x, \mathcal{E}_z)$ is derived from (5.56) by differentiation:

$$\mathcal{E}_x = \hat{\mathcal{E}}_0 \sin(k_x x - \omega t) \exp(-k_x |z|), \tag{5.58a}$$

$$\mathcal{E}_z = \pm \hat{\mathcal{E}}_0 \cos(k_x x - \omega t) \exp(-k_x |z|). \tag{5.58b}$$

This field is depicted in Fig. 5.11 with its surface polarization charges at the crystal-vacuum interface. The type of phonon polariton shown is often called *Fuchs-Kliewer phonon*.

Figure 5.12a exhibits the dielectric function $\epsilon(\omega)$ of an oscillator; this is a good approximation for long-wavelength optical phonons in an IR-active material. The frequencies ω_{TO} and ω_{LO} of the transverse and longitudinal bulk optical phonons are determined by the pole $\mathrm{Re}\{\epsilon(\omega)\}$ and the condition of $\mathrm{Re}\{\epsilon(\omega_{\mathrm{LO}})\} \simeq 0$. According to (5.49) the frequency of the corresponding optical surface phonon ω_{s} is easily found as the frequency at which $\mathrm{Re}\{\epsilon(\omega)\}$ crosses the value -1 on the ordinate. If $\mathrm{Im}\{\epsilon(\omega)\}$ is not negligible in this frequency range, slight shifts in ω_{s} must, of course, be taken into account.

A comparison of Fig. 5.12a and b implies that for the free electron gas, similar arguments apply as for phonons. Indeed bulk density waves of the electron gas, i.e., *plasmon waves* are irrotational ($\mathrm{curl}\boldsymbol{P} = 0$) and their frequency ω_{p} follows from the condition

$$\epsilon(\omega_{\mathrm{p}}) = 0, \tag{5.59}$$

i.e., in the range of negligible $\mathrm{Im}\{\epsilon(\omega)\}$ for $\mathrm{Re}\{\epsilon(\omega_{\mathrm{p}})\} = 0$.

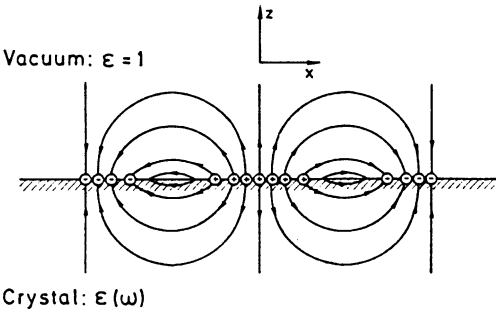

Fig. 5.11 Field distribution of a (Fuchs-Kliewer) surface polariton travelling along the surface (parallel to the x-axis) of an IR-active crystal (semi-infinite half space $z < 0$) described by the dielectric function $\epsilon(\omega)$

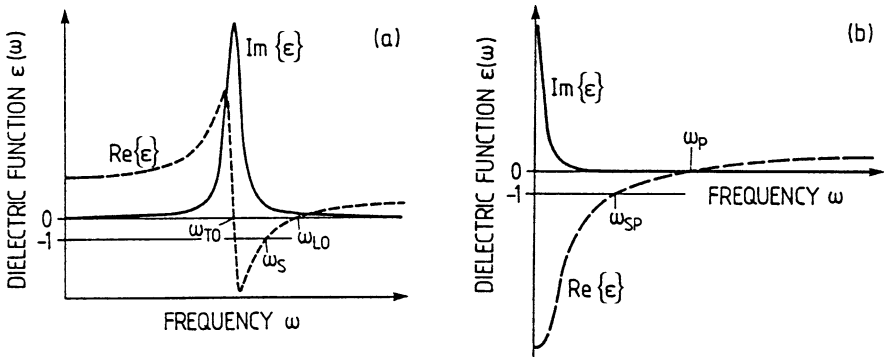

Fig. 5.12 Dielectric functions $\mathrm{Re}\{\epsilon(\omega)\}$ and $\mathrm{Im}\{\epsilon(\omega)\}$ for a harmonic oscillator (**a**) and a free electron gas (**b**). (**a**) In the case of an IR-active crystal, the resonance frequency is the frequency ω_{TO} of the transverse optical (TO) bulk phonon; ω_{LO} is the frequency of the longitudinal optical (LO) bulk phonon, ω_{s} that of the surface phonon polariton. (**b**) ω_{p} is the frequency of the bulk plasmon, case that of the surface plasmon

The same type of analysis as has been performed for phonons can thus be applied to a free electron gas filling a semi-infinite half space bounded by a vacuum interface. However, instead of the dielectric function of the oscillator (eigenfrequency ω_{TO}), one now has to use the dielectric function of a free electron gas (Fig. 5.12b). In the simplest approximation this is a Drude dielectric function

$$\epsilon(\omega) = \epsilon(\infty) - \left(\frac{\omega_{\mathrm{p}}}{\omega}\right)^2 \frac{1}{1 - 1/\mathrm{i}\omega\tau}, \tag{5.60}$$

where

$$\omega_{\mathrm{p}} = \sqrt{\frac{ne^2}{m^*\epsilon_0}} \tag{5.61}$$

is the *plasma frequency* (with n the carrier concentration and m^* the effective mass), and τ the relaxation time. In a better approximation one might apply a Lindhard dielectric function [5.7], or yet more sophisticated methods that take into account the special boundary conditions at a surface [5.8]. The frequency of the surface plasmon ω_{SP} is given, as in (5.49), by the condition

$$\epsilon(\omega_{\mathrm{SP}}) = -1. \tag{5.62}$$

For a Drude dielectric function, by inserting (5.60) into (5.46), one obtains the dispersion relation of *surface plasmon polaritons*

$$\omega^2 = \frac{1}{2}\left[\omega_\mathrm{p}^2 + \left(1 + \frac{1}{\epsilon(\infty)}\right)k_\parallel c^2\right] \times \left[1 - \sqrt{1 - 4\left(\frac{\omega_\mathrm{p}^2 k_\parallel c}{\omega_\mathrm{p}^2 + [1+\epsilon(\infty)^{-1}]k_\parallel^2 c^2}\right)^2}\right]. \tag{5.63}$$

This dispersion relation is displayed in Fig. 5.13. In the case of surface plasmons one has to distinguish between two different cases. In a metal the carrier concentration is on the order of $10^{22}\,\mathrm{cm}^{-3}$, and the corresponding plasmon energies ω_p and ω_SP are on the order of 10 eV. In an n-type semiconductor the plasma frequencies of the valence electrons are of the same order of magnitude ($n \approx 10^{22}\,\mathrm{cm}^{-3}$), but now we have to treat the free electrons in the conduction band separately. For a conduction electron density of typically $10^{17}\,\mathrm{cm}^{-3}$, the corresponding plasmon energies are in the range 10–30 meV. This is exactly the range of typical phonon energies.

An experimental example, in which one can observe both types of surface polaritons, the phonon and the plasmon, is exhibited in Fig. 5.14. High-Resolution Electron Energy Loss Spectroscopy (HREELS) was used to study the clean cleaved GaAs(110) surface. In part (a) of the figure, semi-insulating GaAs, compensated by a high degree of Cr doping, was used. In this material the free-carrier concentration is negligible. Only surface phonons can be expected to occur in the low-energy range up to 200 meV loss energy. The series of energetically equidistant gain and loss peaks indicates multiple scattering on one and the same excitation. The excitation energy is derived from the spacing of the loss peaks as 36.2 ± 0.2 meV. Taking the well-known dielectric function $\epsilon(\omega)$ from IR data for GaAs [5.10] one can calculate the frequency ω_s of the surface phonon polariton by means of (5.49). This calculation yields a value of $\omega_\mathrm{s} = 36.6$ meV in good agreement with the experimental value. A thorough quantum-mechanical theory of the scattering process (Chap. 4) [5.11] predicts that the intensity of the multiple scattering events should be distributed according to a Poisson distribution, i.e.,

$$P(m) = I_m / \sum_\nu I_\nu = (m!)^{-1} Q^m \mathrm{e}^{-Q}, \tag{5.64}$$

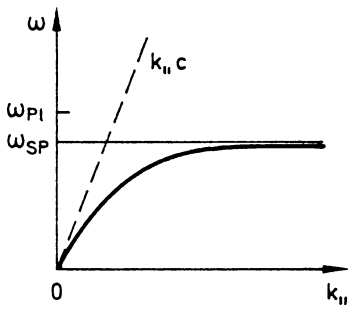

Fig. 5.13 Dispersion curve $\omega(k_\parallel)$ of surface plasmons on a semi-infinite half space containing a free electron gas; $k_\parallel$ is the wavevector parallel to surface; ω_p and ω_SP are the frequencies of bulk and surface plasmons for large $k_\parallel$ (small wavelength)

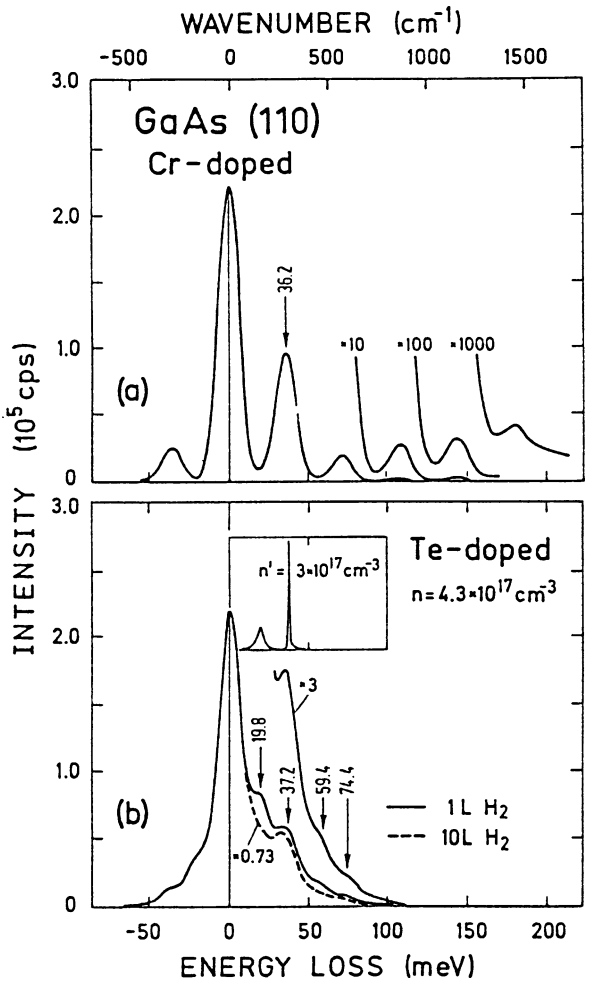

Fig. 5.14 (**a**) Loss spectrum of a clean cleaved GaAs(110) surface of semi-insulating material (angle of incidence 80°). (**b**) Loss spectra measured on an n-type sample after exposure to atomic hydrogen (angle of incidence 70°; H coverage unknown) Inset: Calculated surface loss function $-\mathrm{Im}\{(1+\epsilon)^{-1}\}$ in arbitrary units; $\epsilon(\omega)$ contains contributions from the TO lattice oscillator and from the free electron gas (density $n' = 3 \cdot 10^{17}\,\mathrm{cm}^{-3}$ [5.9]

where I_m is the intensity of the mth loss. Q is the one-phonon excitation probability, i.e., the squared absolute magnitude of the Fourier transform of the time-dependent perturbation due to the scattered electron. This distribution law is well verified as can be seen from Fig. 5.15a.

The scattered electron can not only lose energy by excitation of a surface phonon, but can also gain the same amount of energy by deexcitation of a phonon that is already thermally excited. As in Raman spectroscopy, the gain (I_{-m}) and loss (I_m) intensities (Stokes and anti-Stokes lines) are then expected to be related to each other through a Boltzman factor

$$I_{-m}/I_m = \exp(-m\hbar\omega_s/kT). \tag{5.65}$$

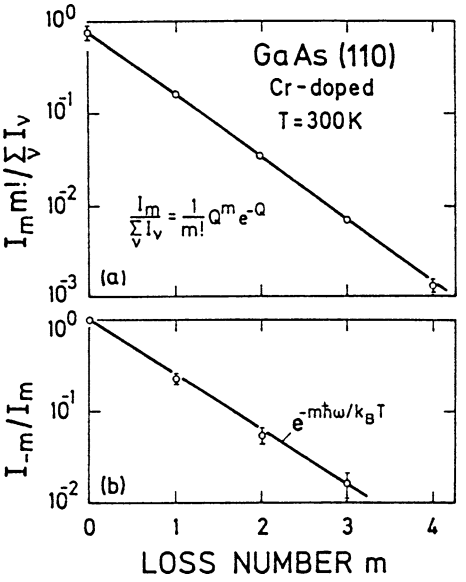

Fig. 5.15 (**a**) Poisson distribution of the loss intensities I_m measured on a clean semi-insulating GaAs surface (Fig. 5.14). (**b**) Intensity ratio of the mth surface phonon gain and the mth phonon loss vs. loss number m. The straight line is calculated with $\hbar\omega = 36.0\,\text{meV}$ [5.9]

This is also found experimentally, as is seen from Fig. 5.15b. On n-doped GaAs with free electron concentrations in the conduction band of 10^{17}–$10^{18}\,\text{cm}^{-3}$ loss spectra like that of Fig. 5.14b are found. On clean cleaved surfaces and also after exposure to small amounts of dissociated hydrogen (or to residual gas) a series of gain and loss peaks is observed at energies $\hbar\omega_+$ (and multiples thereof) resembling those of the surface phonon ($\hbar\omega_\text{s}$). Additional gains and losses (including multiples) are also observed with a significantly smaller quantum energy $\hbar\omega_-$. The spectral position of these peaks is very sensitive to the free-carrier concentration in the bulk and to the gas treatment of the surface. An interpretation in terms of surface plasmons is therefore obvious. A quantitative description of the experimental spectra is possible by assuming a dielectric function for GaAs of the form

$$\epsilon(\omega) = \epsilon(\infty) + [\epsilon(0) - \epsilon(\infty)]\frac{\omega_\text{TO}^2}{\omega_\text{TO}^2 - \omega^2 - \text{i}\omega\gamma} - \left(\frac{\omega_\text{p}}{\omega}\right)^2 \frac{1}{1 - 1/\text{i}\omega\tau}, \quad (5.66)$$

which contains an oscillator contribution due to the TO optical phonons (ω_TO) and a Drude term (5.60) which takes into account the free electrons in the conduction band.

$$\omega_\text{p}^2 = ne^2/\epsilon_0 m_n^* \quad (5.67)$$

is the bulk plasma frequency where n is the free carrier concentration and m_n^* is their effective mass.

$$\tau = m_n^* \mu / e \quad (5.68)$$

is the Drude relaxation time with μ being the mobility. The dielectric function (5.66) is a superposition of the real and imaginary parts depicted in Figs. 5.12a and b.

According to Sect. 4.6 the essential structure of an electron energy loss spectrum is given within the framework of dielectric theory by the surface loss function $\mathrm{Im}\{-1/[\epsilon(\omega)+1]\}$. For monotonic and relatively small $\mathrm{Im}\{\epsilon(\omega)\}$ the maxima are found at the frequencies determined by the condition (5.49). This is also true if one inserts the more complex $\epsilon(\omega)$ of (5.66) into the surface loss function. $\mathrm{Im}\{-1/[\epsilon(\omega)+1]\}$ then exhibits two maxima at frequencies or quantum energies $\hbar\omega_-$ and $\hbar\omega_+$ that correspond to solutions of (5.49). According to (5.66–5.68) these two solutions $\hbar\omega_-$ and $\hbar\omega_+$ depend on the concentration n of free electrons in the conduction band. Figure 5.16 exhibits the calculated loss peak positions (full line), i.e., the energies $\hbar\omega_-$ and $\hbar\omega_+$ as functions of an effective carrier concentration n'. The lower branch $\hbar\omega_-$ has surface-plasmon-like character for small n' whereas $\hbar\omega_+$ is surface-phonon-like. Near $n' = 10^{18}\,\mathrm{cm}^{-3}$ the two branches interchange their character thus indicating a coupling between the two modes via their long-range electric fields. The two frequencies ω_- and ω_+ derive from the values ω_{SP} and ω_s in Fig. 5.12 when the two dielectric functions in Figs. 5.12a and b are superimposed. The combined $\epsilon(\omega)$ exhibits two solutions of $\epsilon(\omega) = -1$ in the regime of negligible $\mathrm{Im}\{\epsilon\}$. In Fig. 5.16 some experimentally determined loss-peak positions are plotted, too. The experimentally determined $\hbar\omega_-$, $\hbar\omega_+$ values after cleavage fit the theoretical curves very well if the effective carrier concentration n' is taken to

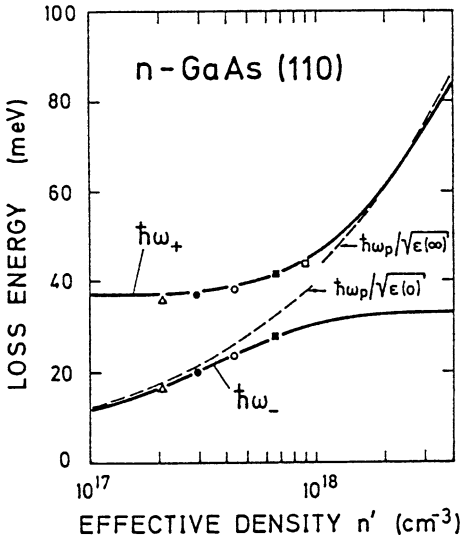

Fig. 5.16 Loss peak positions $\hbar\omega_+$ and $\hbar\omega_-$ calculated from the maxima of the surface loss function with $\epsilon(\omega)$ according to (5.50) (solid lines). Dashed line: plasmon frequency without coupling to surface phonon. The experimental points are measured on samples with different n-type doping: (1) Te-doped (bulk density: $n = 9 \cdot 10^{17}\,\mathrm{cm}^{-3}$): (□) clean, (■) after exposure to 1 L residual gas. (2) Te-doped (bulk density: $n = 4.3 \cdot 10^{17}\,\mathrm{cm}^{-3}$): (○) clean, (●) after exposure to 1 L dissociated H_2. (3) Si-doped (bulk density: $n = 3 \cdot 10^{17}\,\mathrm{cm}^{-3}$): (△) clean [5.9]

be that of the bulk (n), as determined by Hall-effect measurements. After hydrogen treatment, however, the effective carrier concentration n' is reduced as is seen from the positions of the loss peaks (Fig. 5.16). This effect is due to the depletion of carriers in a region of some hundreds of Ångstroms below the surface due to an upwards band bending of the conduction band (space charge region; Chap. 7). This so-called *depletion layer* is induced by hydrogen adsorption. It influences the loss peak position since the positions $\hbar\omega_+$ and $\hbar\omega_-$ are determined by carrier concentration within the penetration depth $1/q_\parallel$ of the electric field of the surface phonon and plasmon-like excitations. From the relation $q_\parallel \simeq \hbar\omega/2E_0$ (4.42) this penetration depth is also estimated to be about a couple of hundred Ångstroms. The measurement of surface phonon/plasmon excitations can therefore be used to investigate carrier concentrations in space charge layers at semiconductor interfaces and surfaces [5.12] (Chap. 7).

5.6 Dispersion Curves from Experiment and from Realistic Calculations

When the wavelength of surface waves is comparable to the interatomic separation of the discrete crystal lattice, the continuum-type approach of the preceding sections is no longer valid. For frequencies on the order of $10^{11}\,\mathrm{s}^{-1}$ or higher, the description of surface modes demands a lattice dynamical approach. This requires, as in bulk lattice dynamics, a detailed knowledge of the interatomic force constants. For appropriate approximations the effects of electron-lattice interactions have to be taken into account by means of shell models, in which the valence electrons are represented by a solid shell bound to the core by a spring. In even more sophisticated treatments, deformations of the electron shell itself can be taken into account by so-called *breathing shell models*. Compared to bulk lattice dynamics a fundamental new problem arises at the surface: due to reconstruction or relaxation of the topmost atomic layers, both the atomic geometry and the restoring forces may deviate near the surface from their bulk values. These changes are not generally known. They give rise to additional parameters which must be fitted to experimental data.

A variety of lattice-dynamical techniques have been applied to calculate surface phonon dispersion branches. An approach frequently used in the past is the analogy of the continuum approach (Sect. 5.3): a trial solution is constructed for the semi-infinite lattice and, by means of the correct boundary conditions, dispersion curves are obtained. It is not always clear whether all possible surface modes are obtained by this calculation. Another method consists of the direct calculation of the eigenvalues and polarization vectors of a slab formed by a sufficiently large number of atomic layers. This method yields all the acoustic and optical surface modes over the entire Brillouin zone, provided that their penetration depth is less than the slab thickness. In many cases twenty layers are enough to give good results. A third method is based on the application of Green's function theory. In this approach the surface is treated as a perturbation which modifies the spectrum of bulk vibrations.

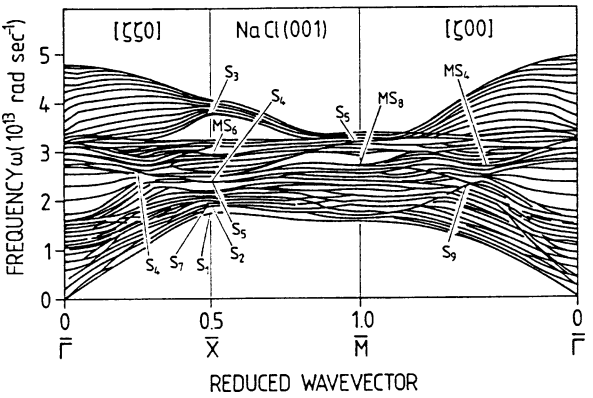

Fig. 5.17 Dispersion curves of a 15 layer (001)-oriented NaCl slab obtained from a shell model calculation. The finite number of slabs gives rise to a discrete set of dispersion curves. The dispersion branches labeled by S_1, S_2 ... etc. belong to vibrational eigenvectors which decay into the bulk, i.e., they describe surface phonons. [5.13]

Figure 5.17 shows an example of results obtained from a slab calculation for NaCl(001) [slab orientation (001)]. Corresponding to the finite number of slabs (15) the bulk modes are obtained as a discrete set of dispersion curves. With increasing number of the slabs these bulk modes thicken to form quasi-continuous areas, i.e. bands. However, a finite number of modes labeled S_1, S_2, S_3 etc., remain distinct from the bands. Their eigenvectors are found to be large near the surface and rapidly decreasing, away from the surface. These modes can obviously be identified as surface vibrations. The acoustic surface mode S_1 is localized beneath the bulk acoustic band, even in the long wavelength limit ($\boldsymbol{k}_\parallel \to \mathbf{0}$). This mode therefore represents the Rayleigh surface waves discussed in Sect. 5.3. The modes S_3, S_4 and S_5 are examples of optical surface vibrations. S_4 and S_5 are the so-called *Lucas modes* with polarization normal and parallel to the surface. These modes are related to the altered force constants between the topmost atomic layers; their vibrational amplitude is therefore strongly localized near the first layer.

As an example of a calculation using the Green's function perturbation method, Fig. 5.18 shows dispersion branches of surface phonons on LiF (001). The outer atomic electrons are modelled by the so-called *breathing shell model*, in which deformations of the shell are explicitly taken into account. Accordingly there is very good agreement between the calculated bulk phonon dispersion branches (shaded area) and some branches that have been determined experimentally by inelastic neutron scattering (black dots). In the plot of Fig. 5.18 the bulk modes with polarization normal ($\perp$) and parallel ($\parallel$) to the (001) surface are shown separately. Some surface phonon bands are marked by S_3, S_4, etc. S_4 and S_5 are again the Lucas modes. They are energetically degenerate with bulk modes polarized normal to the surface and are thus called surface resonances. As is expected from continuum theory (Sect. 5.3), the Rayleigh mode S_1 has frequencies (energies) below those of the bulk modes along the entire symmetry line $\overline{\Gamma M}$. This S_1 band has been calculated by both the Green's function method (full line) and by the slab method (dashed line). There is a small discrepancy near the $\overline{M}$ point which could probably be eradicated if the surface change in ionic polarizibility and/or the anharmonicity were taken into account.

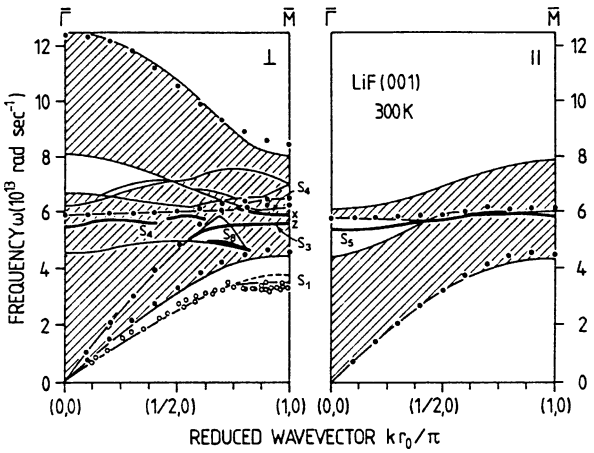

Fig. 5.18 Phonon dispersion branches of LiF(001) along (100) calculated by the Green's function method [5.14]. The bulk modes (shaded area) with polarization normal (⊥) and parallel (∥) to the (001) surface are shown separately. The surface phonon modes are labeled by S_i. For comparison some experimentally determined bulk modes (from neutron scattering) are given as black dots. The open dots (near S_1) are experimental results for the Rayleigh modes, as determined by inelastic atom scattering [5.15]

The theoretical dispersion curve of the Rayleigh mode S_1 calculated using the Green's functions method is in very good agreement with the experimental results from inelastic atom scattering by Brusdeylins et al. [5.15] (Fig. 5.18, open circles). In these experiments a supersonic nozzle beam of He atoms is inelastically scattered on the LiF(001) surface prepared in UHV, and the energy distribution of the backscattered He atoms is measured by a time-of-flight spectrometer (Panel X: Chap. 5). The energy loss at the surface and the scattering angle with respect to the specular beam and the sample surface determine the phonon frequency ω and the transfer, i.e. the dispersion relation $\omega(\boldsymbol{q}_\parallel)$ for the particular surface excitation mode. Rayleigh waves usually produce the strongest peaks in the time of-flight spectra of the scattered atoms due to their large amplitude in the topmost layer.

Surface phonon dispersion branches can also be measured by the inelastic scattering of slow electrons (Panel IX: Chap. 4). In order to measure $\hbar\omega(\boldsymbol{q}_\parallel)$ throughout the whole 2D Brillouin zone, sizeable $\boldsymbol{q}_\parallel$ transfers have to be achieved and the measurement must thus be performed with off-specular scattering geometry. Unlike the case of optical surface phonon polaritons with $\boldsymbol{q}_\parallel \simeq \boldsymbol{0}$ studied in the dielectric scattering regime (Sect. 5.5), the scattering is now predominantly due to short-range atomic potentials. The inelastic scattering cross section for this kind of scattering on phonons rises with increasing primary energy. The HREELS experiments on Ni(100) (Fig. 5.19) were therefore performed with impact energies of 180 and 320 eV in preference to lower energies. The spectra shown in Fig. 5.19 were measured with a resolution of 7 meV in off-specular scattering geometry as shown in the inset of Fig. 5.20. Electrons were collected at a fixed polar angle of $\approx 72°$ along the [110] azimuth ($\overline{\Gamma X}$ direction) while the impinging beam was

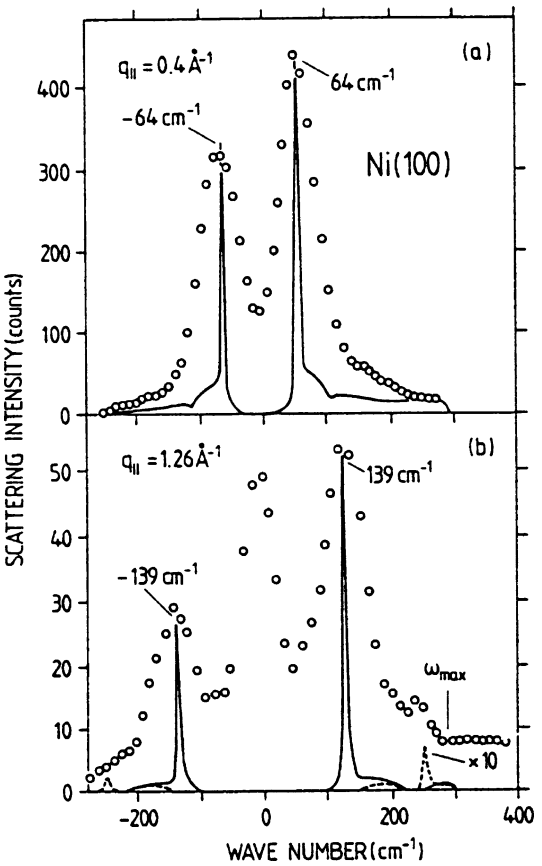

Fig. 5.19 a,b Electron energy loss spectra measured by HREELS with 7 meV energy resolution in off-specular geometry between the (00) and (01) Bragg diffraction beams on the clean Ni(100) surface (geometry as in inset of Fig. 5.20). (**a**) for a wavevector transfer $q_{\parallel}$ of $0.4\,\text{Å}^{-1}$; (**b**) for a wave vector transfer $q_{\parallel}$ of $1.26\,\text{Å}^{-1}$; experimental data points (open circles), calculated spectra (solid lines) [5.16]

rotated between polar angles yielding the (01) and (00) Bragg-diffracted beams. The momentum resolution was $\Delta q_{\parallel} \approx 0.01\,\text{Å}^{-1}$. Phonon losses were found over the entire range between the (01) and (00) positions. The particular $q_{\parallel}$ transfer of $1.26\,\text{Å}^{-1}$ in Fig. 5.19b corresponds to the $\overline{X}$ point of the 2D Brillouin zone. The experimental data (open circles) are compared with a calculation based on a nearest-neighbour central-force model in which the force constant between first and second layer is stiffened by 20%. The calculated curves show the frequency spectrum of phonons with displacements normal to the surface for the corresponding $q_{\parallel}$ wave vectors, for atoms in the outermost substrate layer. The wings on the high-frequency side of the surface phonon loss originate from the bulk phonon continuum.

The experimental peak positions as a function of $q_{\parallel}$ [calculated according to (4.41)] are plotted in Fig. 5.20. The measured dispersion coincides closely with that calculated by Allen et al. [5.17] for a surface phonon on Ni(100) with an atomic displacement at $\overline{X}$ that is normal to the surface in the outmost layer. According to this calculation there exists a further shear-polarized surface phonon at $\overline{X}$ with displacement parallel to the surface and normal to $\boldsymbol{q}_{\parallel}$. Since for this phonon the

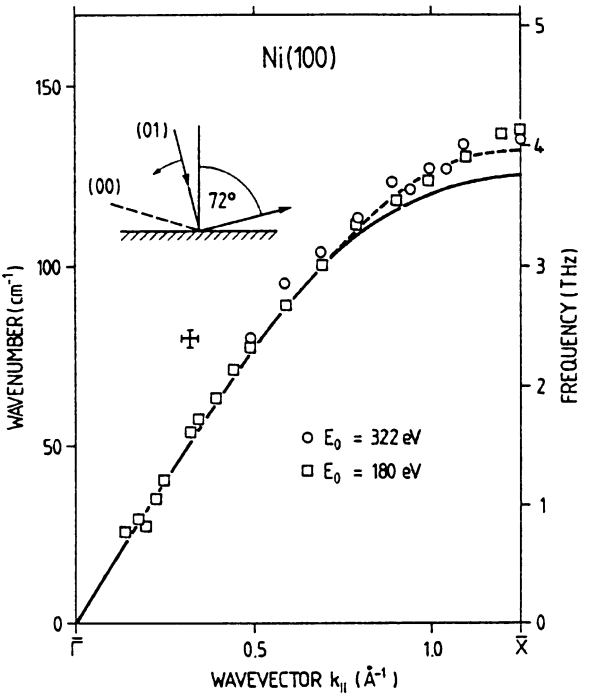

Fig. 5.20 Experimentally determined (HREELS, Fig. 5.19) dispersion of surface phonons on a clean Ni(100) surface (open symbols for two different primary energies E_0). The scattering geometry is shown in the inset (off-specular scattering). The full curve is the calculated dispersion according to Allen et al. [5.17]. The dashed line takes into account a stiffening of the force constants between the topmost and the second atomic layers [5.16]

displacement direction is always normal to $\boldsymbol{K}_\parallel = \boldsymbol{k}'_\parallel - \boldsymbol{k}_\parallel$ the selection rules (4.17)) forbid an excitation in the present scattering geometry (inset of Fig. 5.20). Indeed, this phonon is not observed in the HREELS data.

The agreement between the calculated dispersion (Fig. 5.20, full line) and the data points is poorer near the $\overline{X}$ point. The agreement is improved (dotted line) if the force constant which couples atoms in the first and second layers is increased by 20%. This stiffening of the force constant mimics a modest inward relaxation of the surface atomic layer, which is indeed confirmed by other experiments.

The examples of Li(001) and Ni(100) show that measurements of surface-phonon dispersion curves and a comparison with lattice-dynamical calculations can provide interesting information about changes in force constants and atomic locations near the surface.

Panel X
Atom and Molecular Beam Scattering

Atoms and molecules such as He, Ne, H_2, D_2, impinging on a solid surface as neutral particles with a low energy (typically $< 20\,\text{eV}$), cannot penetrate into the solid. Scattering experiments with neutral particle beams therefore provide a probe that yields information exclusively about the outermost atomic layer of a surface. Such experiments have now become an important source of information in surface physics. Both elastic and inelastic scattering can be studied. A schematic overview of the various scattering phenomena is given in Fig. X.1. Since He atoms, for example, with a kinetic energy of 20 meV have a de Broglie wavelength of 1 Å, scattering phenomena must be described in the wave picture (Sect. 4.1). A particle approaching the surface interacts with the surface atoms through a typical interatomic or intermolecular potential $V(\boldsymbol{r}_\parallel, z)$, $\boldsymbol{r}_\parallel$ being a vector parallel to the surface, and z the coordinate normal to the surface. $V(z)$ consists of an attractive and a repulsive part (as in chemical bonding). The scattering from a two-dimensional periodic lattice of atoms (surface) is dominated by the specular quasi-elastic peak (intensity I_{00}) and elastic Bragg diffraction (intensity I_{hk}) in well-defined directions (as in LEED, Sect. 4.2). This elastic scattering is adequately described in the rigid-lattice

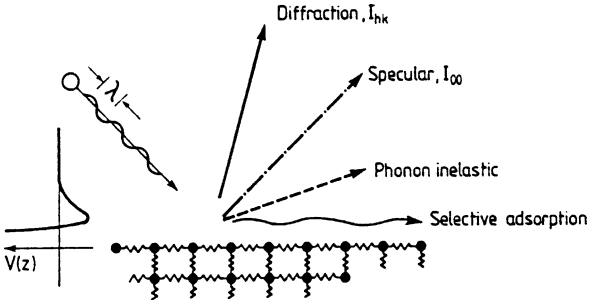

Fig. X.1 Schematic diagram showing the different collision processes that can occur in the non-reactive scattering of a light atom with the de Broglie wavelength comparable to the lattice dimensions. Since the lattice vibrational amplitudes are small, phonon inelastic scattering is expected to be weak relative to elastic diffraction (specular beam I_{00} and Bragg diffraction beams I_{hk}). Additionally, high energy losses can lead to selective adsorption of impinging atoms in the attractive part of the surface atom potential $V(z)$ [X.1]

approximation with only an intensity correction for inelastic effects, provided by the temperature-dependent Debye-Waller factor. An incident atom or molecule can lose so much energy that it is trapped at the surface or "selectively adsorbed". This trapping of atoms in bound states on the surface can strongly modify the scattered intensities at specific angles and energies.

Inelastic scattering comes into play due to the fact that the crystal is in reality not rigid: the atoms vibrate about their average positions. The incident particle can therefore transfer part of its kinetic energy to the dynamic modes of the vibrating surface, the *surface phonons*. Similarly, it can gain energy via the annihilation of a surface phonon.

The mathematical description of the scattering is analogous to that of electron-surface scattering (Sect. 4.1). The most general interaction potential $V(\boldsymbol{r})$ between the incident particle and the crystal surface (4.1) which enters the formula for the scattering cross section (4.17) is conveniently written as a function of $\boldsymbol{r}_\parallel$, a coordinate parallel to the surface, the coordinate z normal to the surface, and $\boldsymbol{s_n}(t)$ the vibrational coordinate of the nth surface atom:

$$V[\boldsymbol{r}_\parallel, z, \boldsymbol{s_n}(t)] = V(\boldsymbol{r}_\parallel, z)|_{\boldsymbol{s_n}=0} + \sum_{\boldsymbol{n}} (\nabla V) \cdot \boldsymbol{s_n}(t) + \ldots . \tag{X.1}$$

The first term in the potential expansion is the corrugated elastic potential, which can be determined by fitting the intensities of the elastic diffraction peaks using model potentials. Elastic scattering thus yields information about the topology of the surface and about details of the interatomic potentials. The second- and higher-order terms, which couple to the vibrations $\boldsymbol{s_n}(t)$ of the surface atoms, are responsible for inelastic scattering. An understanding of these coupling terms is fundamental for an interpretation of such phenomena as sticking coefficients (Sect. 9.5) and energy transfer between surface atoms and incident particles.

Before presenting some detailed examples of the application of atom scattering, the experimental set-up will be discussed briefly.

The experimental apparatus consists of a source of monoenergetic molecules or atoms which are directed as a beam towards the surface under investigation; the back-scattered distribution is recorded by a detector. Both sample and detector can be rotated around a common axis in the surface plane to allow the detection of higher diffraction orders under different angles. Since neutral particles are used, neither electric nor magnetic fields can be used as focussing or dispersive elements. A schematic diagram of a typical experimental set-up is shown in Fig. X.2. An important feature is the nozzle beam source producing the monochromatic rare-gas beam. The beam of Ne or He atoms is produced in a high-pressure expansion source. In the expansion of the gas from a source pressure of about 2 atm through a thin-walled orifice (diameter $\approx 5 \cdot 10^{-2}$ mm) to a beam pressure of about 10^{-4} Torr, the random translational energy is converted into a forward mean velocity of the beam. Thus the magnitude of the random velocity component which determines the velocity spread Δv is reduced relative to the most probable velocity v. In the apparatus shown in Fig. X.2 the resultant $\Delta v/v$ is about 10%. With improved nozzle

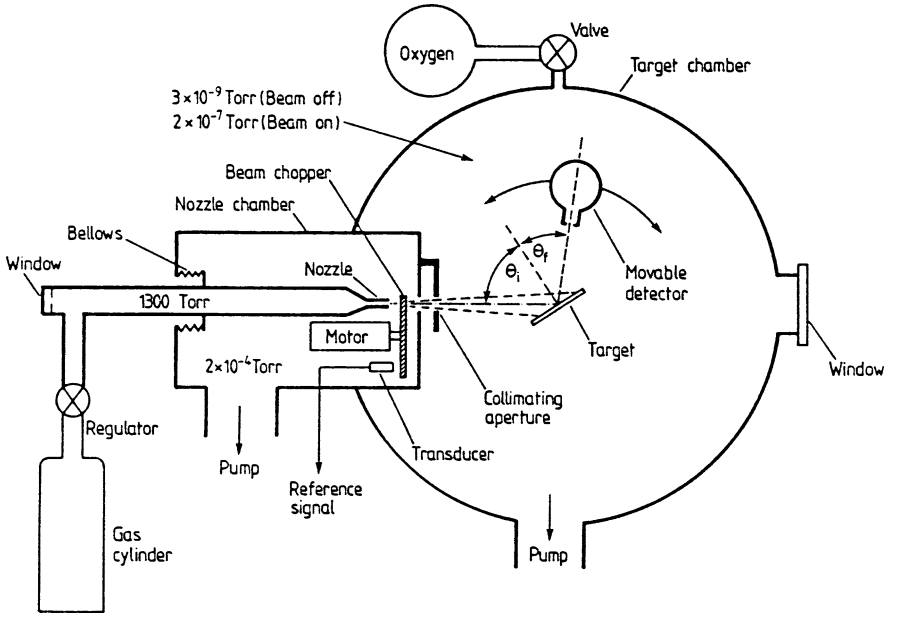

Fig. X.2 Schematic diagram of a typical low-energy molecular beam scattering apparatus [X.2]

beam sources $\Delta v/v$ values on the order of 1% are achieved. Toennies [X.3] used a He source cooled down to 80 K. The beam is expanded from a pressure of 200 atm through a 5 μm hole into vacuum. To improve the forward velocity distribution further, the beam passes a skimmer after expansion. This funnel-shaped tube skims off atoms with insufficiently forward-directed velocity. During the expansion, chaotic thermal motion is converted into a concerted forward motion of the atoms and as a result of enthalpy conservation, the temperature in the moving gas is drastically reduced; behind a distance of about 20 mm to $\approx 10^{-2}$ K. This corresponds to a relative velocity spread of less than 1%. With modern nozzle-beam sources, primary energies from 6 meV up to 15 eV can be produced. He atoms with de Broglie wavelengths of 1 Å have an energy of about 20 meV. In Fig. X.2 the primary beam is modulated by a chopper and phase-sensitive detection is employed using a lock-in amplifier. This technique allows detection of the modulated scattered beam against a relatively high background pressure. Either standard ion gauges or more sophisticated mass spectrometers are employed as detectors.

In the following, some examples are presented of the different applications of atom and molecular scattering based on the processes of Fig. X.1. Since He atoms are essentially scattered on the almost structureless "electron sea", far from the uppermost surface lattice plane, an ideal well-ordered, close-packed metal surface gives rise to virtually no interesting scattering phenomena. But deviations from ideality, such as steps, defects or adsorbates, can affect the elastically scattered intensity in reflection direction, i.e. the specular beam intensity I_{00} quite dramatically. Figure X.3 shows the intensity variation of the specular beam of He atoms

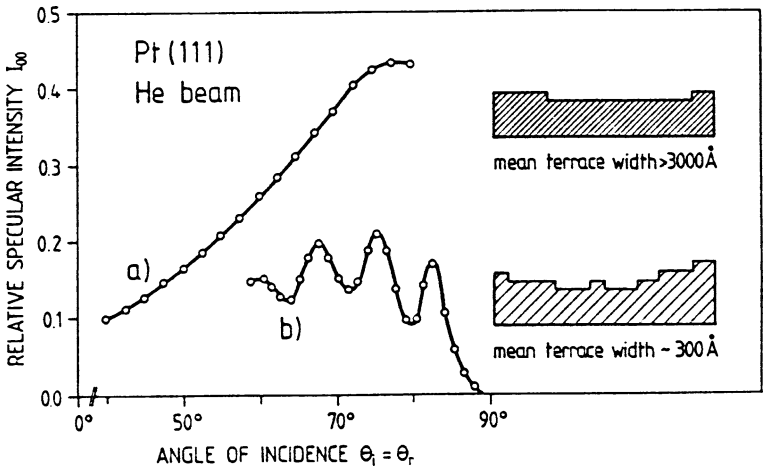

Fig. X.3 Relative specular intensity I_{00} (referred to primary beam intensity) of a low-energy He atom beam (energy $E = 63$ meV) versus angle of incidence θ_i ($= \theta_r$ reflection angle) for two Pt(111) surfaces with differing average terrace widths [X.4]

reflected from Pt(111) surfaces with differing distributions of steps and terraces. For the measurement the angle of incidence $\theta_i (= \theta_r)$ is varied over a small range and the backscattered intensity I_{00} is recorded. For this purpose, of course, an experimental set-up with detection under variable observation direction is necessary. According to the differing terrace width (average values around 300 Å and above 3000 Å) an interference pattern or an essentially monotonic variation is observed in the angular region considered. The oscillations are explained in terms of constructive and destructive interferences of the He wave function reflected from (111) terraces which are separated by monatomic steps. The average terrace width, i.e., the step density, determines similarly as in an optical grid slit width and distance, the phase differences of the evading He waves under certain observation directions. The oscillation period of curve (b) allows an estimation of the step atom density of about 1%. Better preparation techniques lead to step atom densities lower than 0.1% which then give rise to a higher total reflection intensity, and the interference oscillations are absent (curve a). The technique is thus useful for characterizing the degree of ideality of a clean surface after preparation.

Elastic He atom scattering, i.e. diffraction, can provide information about the structural properties of a surface. In contrast to electron scattering in LEED (Panel VIII: Chap. 4), where the electrons penetrate several Ångstroms into the solid, only the outermost envelope of the electron density about the surface is probed by the He atoms. This makes the technique relatively insensitive to clean, well-ordered, densely-packed metal surfaces; but ordered adsorbate atoms or molecules whose electron density protrudes significantly from the surface, give rise to stronger scattering intensities in certain Bragg spots. This is shown for the example of a

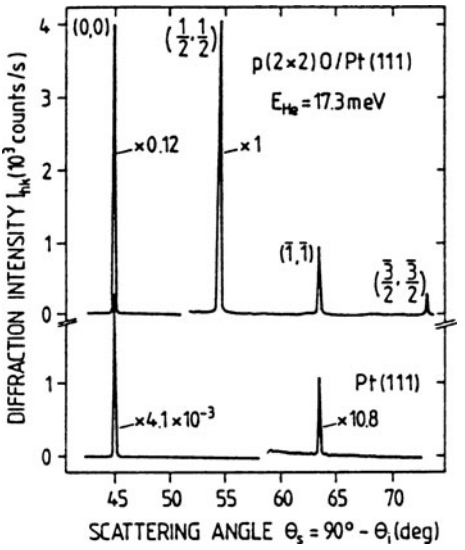

Fig. X.4 He-beam polar diffraction patterns in the [112] direction from the clean (bottom) and p(2 × 2)O/Pt(111) oxygen covered surface (top). The primary He energy E_{He} is 17.3 meV and the sample temperature 300 K [X.5]

well-ordered oxygen layer with p(2 × 2) superstructure on Pt(111) in Fig. X.4. For the clean Pt surface the ($\bar{1}$, $\bar{1}$) Bragg spot has ten times less intensity than on the oxygen covered surface. The diffraction spots ($\bar{1}$/2, $\bar{1}$/2) and ($\bar{3}$/2, $\bar{3}$/2) due to the oxygen superlattice occur with much higher intensity. Adsorbate effects are thus clearly distinguished from substrate spots and the interpretation problems sometimes encountered for adsorbate LEED patterns (substrate vs. adsorbate superstructure) do not exist. The method of atom and molecule diffraction is therefore complementary to LEED because of its extreme sensitivity to the outermost atomic layer. In the inelastic scattering regime, atom and molecule scattering from surfaces also provides interesting advantages over other scattering techniques because of its high energy resolution. Because the possible energy and wave vector transfer are well matched throughout the whole Brillouin zone, surface-phonon dispersion branches (Chap. 5) can be measured with extremely high accuracy. Figure X.5 shows inelastic He beam spectra measured with different angles of incidence θ_i on Cu(110). The detection direction is chosen for wave-vector transfers along $\overline{\Gamma Y}$. The experimental resolution readily allows the determination of peak half-widths below 1 meV. Thus information about broadening due to phonon coupling etc. can also be derived from the experimental data. This is by no means possible from electron scattering data (HREELS, Panel IX: Chap. 4), where the best energy resolution is on the order of 1 meV. Surface phonon dispersion curves derived from spectra such as those of Fig. X.5 are given in Fig. X.6, but here along the $\overline{\Gamma X}$ direction of the Cu(110) surface Brillouin zone. The data denoted by R correspond to the Rayleigh surface waves (Chap. 4).

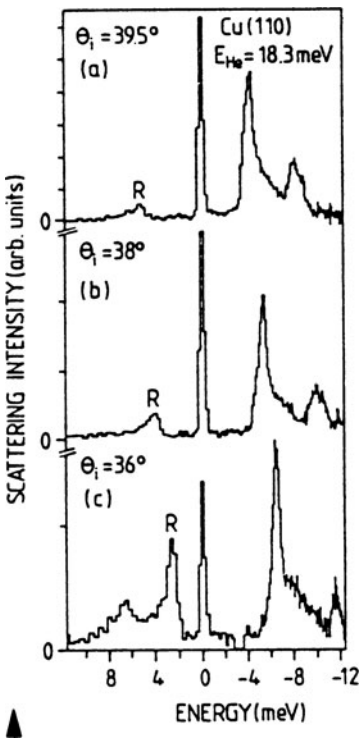

Fig. X.5 Inelastic He scattering spectra taken along the $\overline{\Gamma X}$ direction of the surface Brillouin zone on Cu(110). The primary He beam energy is 18.3 meV [X.6]

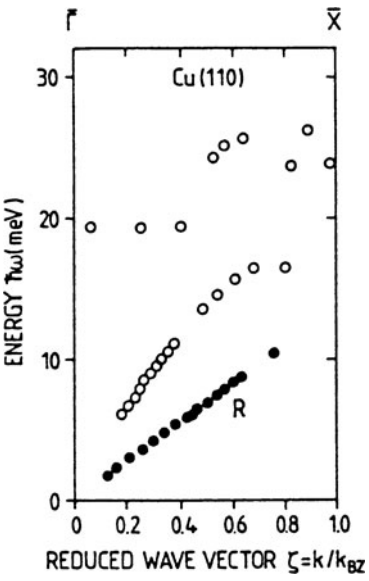

Fig. X.6 Surface phonon dispersion curves as obtained by inelastic He scattering (primary energy $E_{\mathrm{He}} = 18.3\,\mathrm{eV}$) along the $\overline{\Gamma Y}$ direction of the surface Brillouin zone on Cu(110). The reduced wave vector ξ is defined by $\xi = k/k_{\mathrm{BZ}}(\overline{X})$ with $k_{\mathrm{BZ}}(\overline{X}) = 1.23\,\mathrm{\AA}^{-1}$ as the Brillouin-zone dimension in the $\overline{X}$ direction [X.6]

References

X.1 J.P. Toennies: Phonon interactions in atom scattering from surfaces, in *Dynamics of Gas-Surface Interactions*, ed. by G. Benedek, U. Valbusa, Springer Ser. Chem. Phys. Vol. 21 (Springer, Berlin, Heidelberg 1982) p. 208
E. Hulpke (ed.): *Helium Atom Scattering from Surfaces*, Springer Ser. Surf. Sci., Vol. 27 (Springer, Berlin, Heidelberg 1992)
X.2 S. Yamamoto, R.E. Stickney: J. Chem. Phys. **53**, 1594 (1970)
X.3 J.P. Toennies: Physica Scripta T**1**, 89 (1982)
X.4 B. Poelsema, G. Comsa: *Scattering of Thermal Energy Atoms from Disordered Surfaces*, Springer Tracts Mod. Phys., Vol. 115 (Springer, Berlin, Heidelberg 1989)
X.5 K. Kern, R. David, R.L. Palmer, G. Comsa: Phys. Rev. Lett. **56**, 2064 (1986)
X.6 P. Zeppenfeld, K. Kern, R. David, K. Kuhnke, G. Comsa: Phys. Rev. B **38**, 12329 (1988)

Problems

Problem 5.1 Information can be transmitted through a solid by bulk sound waves or by Rayleigh surface waves. What phonons provide a faster transmittance velocity? Discuss the problems which arise for the signal propagation by means of short pulses when long wavelengths $\lambda \gg a$ (lattice parameter) and short wavelengths $\lambda \approx a$ are used.

Problem 5.2 The dielectric response of an infrared active, n-doped semiconductor is described in the IR spectral region by a dielectric function ϵ (5.66) which contains an oscillator contribution due to TO phonons (5.50) and a Drude-type contribution (5.60) due to free electrons in the conduction band. Calculate the surface loss function $\mathrm{Im}\{-1/[\epsilon(\omega) - 1]\}$ and discuss the loss spectrum expected in an HREELS experiment as a function of carrier concentration. Flat-band situation is assumed at the surface.

Problem 5.3 Surface phonon polaritons (Fuchs-Kliewer phonons) are excited on a clean GaAs(110) surface in an HREELS experiment with a primary energy of 5 eV. Calculate from the corresponding loss peak at 36.2 meV the exponential decay length of the polarisation field of the surface phonons. Discuss the consequence for an HREELS measurement which is performed on a GaAs film which is thinner than the calculated decay length.

Problem 5.4 Calculate the frequency of a surface phonon on the (100) surface of an fcc crystal at the Brillouin-zone boundary in the [110] direction. Only central forces between next neighbour atoms are assumed. The surface phonon should have odd symmetry with respect to the mirror plane defined by the phonon wave vector $\boldsymbol{q}$ and the surface normal.
Why is the calculation so simple?
Does a second surface phonon exist on this surface which is localized on the first atomic monolayer?